

A. N. Petrov · V. A. Cherepanov · A. Yu. Zuev

Thermodynamics, defect structure, and charge transfer in doped lanthanum cobaltites: an overview

Received: 17 January 2006 / Accepted: 31 January 2006 / Published online: 4 May 2006
© Springer-Verlag 2006

Abstract This work, based on the experimental and theoretical research performed by the authors during last three decades, presents an overview of phase and defect thermodynamics, electronic transport properties, and the stability of cobaltite-based mixed conductors that are promising for electrode and membrane applications. Attention is centered on (1) the phase equilibria in La-Me-Co-T-O (where Me=Ca, Sr, Ba and T=Mn, Fe, Ni, Cu) systems and crystal structure of the complex oxides formed in these systems, thermodynamic stability and the homogeneity ranges of solid solutions; (2) the defect structure of the oxygen-deficient undoped and acceptor- or/and donor-doped lanthanum cobaltites; and (3) their conductivity and Seebeck coefficient as functions of temperature and oxygen partial pressure. The relationships between the peculiarities of the defect structure and the transport properties of the lanthanum cobaltites with different dopant natures are analyzed.

Keywords Cobaltite · Mixed conductor · Defect structure · Defect thermodynamics · Electrode · Membrane

Introduction

Lanthanum cobaltite doped with the alkali earth elements (Ca, Sr, Ba) on A-site and 3d-transition metals (Mn, Fe, Ni, Cu) on B-site $\text{La}_{1-x}\text{Me}_x\text{Co}_y\text{T}_z\text{O}_{3\pm\delta}$ exhibit unique

properties enabling the use of these materials as catalysts for various oxidation-reduction reactions, oxygen membranes, or electrodes for different electrochemical devices (solid oxide fuel cells, batteries, CO₂-lasers, and so on). The first-priority goal of the present paper, based mainly on experimental and theoretical work performed by the authors during last three decades, was to give an overview on the phase equilibria in La-Me-Co-T-O (where Me=Ca, Sr, Ba and T=Mn, Fe, Ni, Cu) systems and the crystal structure of the complex oxides formed in these systems. Secondly, the question as to how the alteration of the defect structure caused by doping $\text{LaCoO}_{3-\delta}$ with acceptor dopant (Sr) on A site and both acceptor (Cu) and donor dopant (Mn) on B site affects the charge transfer in this oxide was addressed. To answer this question, an analysis of combined data on the oxygen nonstoichiometry, electronic conductivity, and Seebeck coefficient as functions of temperature and oxygen partial pressure was carried out for undoped $\text{LaCoO}_{3-\delta}$ and its derivatives, such as $\text{La}_{1-x}\text{Sr}_x\text{Co}_{3-\delta}$ ($x=0.3$ and 0.6), $\text{La}_{0.7}\text{Sr}_{0.3}\text{Co}_{0.75}\text{Mn}_{0.25}\text{O}_{3-\delta}$, and $\text{LaCo}_{0.7}\text{Cu}_{0.3}\text{O}_{3-\delta}$.

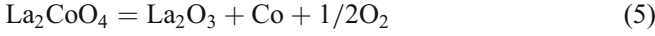
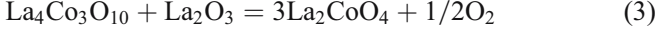
Thermodynamics

Quasibinary systems

Phase equilibria The phase equilibria in the parent La-Co-O system and thermodynamic properties of the ternary oxides formed in this system have been studied in detail [1–5]. In the parent system, there are three complex oxides, LaCoO_3 , $\text{La}_4\text{Co}_3\text{O}_{10}$, and La_2CoO_4 , with the perovskite-related structure, which can be described by the general formula $\text{La}_{n+1}\text{Co}_n\text{O}_{3n+1}$. The mean oxidation state of cobalt ions in these complex oxides decreases in the raw while n decreases. This is in conformity with phase

A. N. Petrov · V. A. Cherepanov (✉) · A. Y. Zuev
Chemical Department, Ural State University,
Lenin Av. 51, 620083 Yekaterinburg, Russia
e-mail: vladimir.cherepanov@usu.ru
Tel.: +7-3432-615412

transformations, which take place (at constant temperature) step by step while oxygen pressure decreases:



Stability ranges of each phase can be shown by different cross-sections of the phase diagram of the La–Co–O system shown in Figs. 1, 2, and 3. Because most promising materials are based on LaCoO_3 , it is important to compare stability ranges of this complex oxide with LaTO_3 , where T is another 3d-transition metal. The thermodynamic stabilities of lanthanum manganite, lanthanum ferrite, lanthanum cobaltite, and lanthanum nikelite, studied using the electromotive force technique and thermogravimetric analysis (TGA) [2–4, 6–10], are presented in Table 1. In general, with the exception of LaFeO_3 , the thermodynamic stability decreases with the increase of the 3d-transition metal atomic number. It was

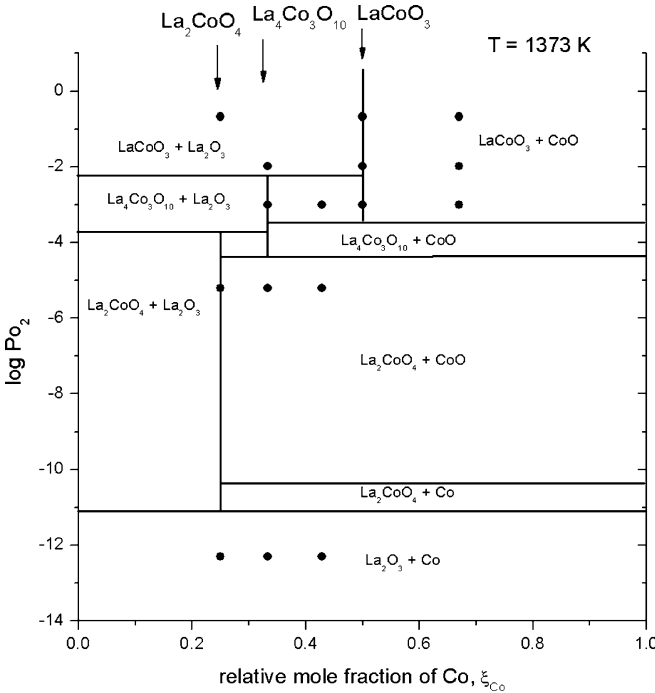


Fig. 1 Isothermal cross-section of the phase diagram for the La–Co–O system

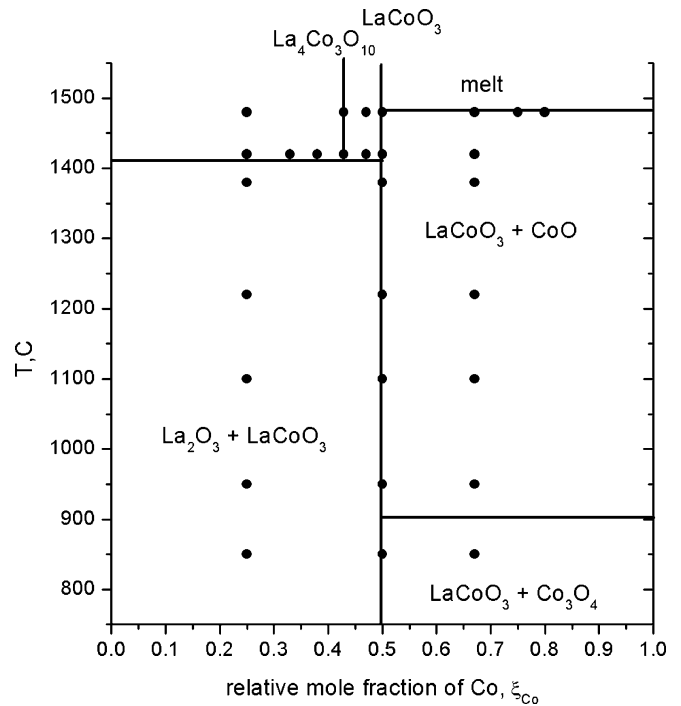


Fig. 2 Isobaric ($p_{\text{O}_2}=0.21$ atm) cross-section of the phase diagram for the La–Co–O system

shown that the specific features of the $3d^n$ configuration of transition metal, together with the ability of the formation of other related phases, govern the stability of the perovskite structure [11].

Crystal structure Lanthanum cobaltite LaCoO_3 possesses a rhombohedrally distorted perovskite lattice. The crystal structure of the so-called Ruddlesden–Popper phases $\text{La}_{n+1}\text{Co}_n\text{O}_{3n+1}$ can be described as an alternation of n perovskite blocks with rock salt layers. Perovskites with other 3d-transition metals are also distorted: LaMnO_3 and LaFeO_3 —orthorhombically ($Pbnm$ space group)—and LaNiO_3 —rombohedrally ($R\bar{3}c$ space group), as for lanthanum cobaltite.

Ternary systems

La–Me–Co–O systems (Me=Ca, Sr, Ba)

The introduction of alkali earth metal to the La–Co–O system leads to the formation of two types of solid solutions: $\text{La}_{1-x}\text{Me}_x\text{CoO}_{3-\delta}$ and $(\text{La}_{1-x}\text{Me}_x)_2\text{CoO}_4$. Although La_2CoO_4 is not stable in air, partial substitution of La^{3+} for Me^{2+} increases the mean oxidation state of cobalt ions and stabilizes the K_2NiF_4 structure in some ranges of Me-content even in air [12–15]. Partial substitution of La^{3+} for Me^{2+} in $\text{La}_{1-x}\text{Me}_x\text{CoO}_{3-\delta}$ is accompanied with an increase of mean oxidation state of cobalt ions and a significant increase of oxygen deficiency. Detailed analysis of oxygen nonstoichiometry will be shown further, but one should mention here that in the first

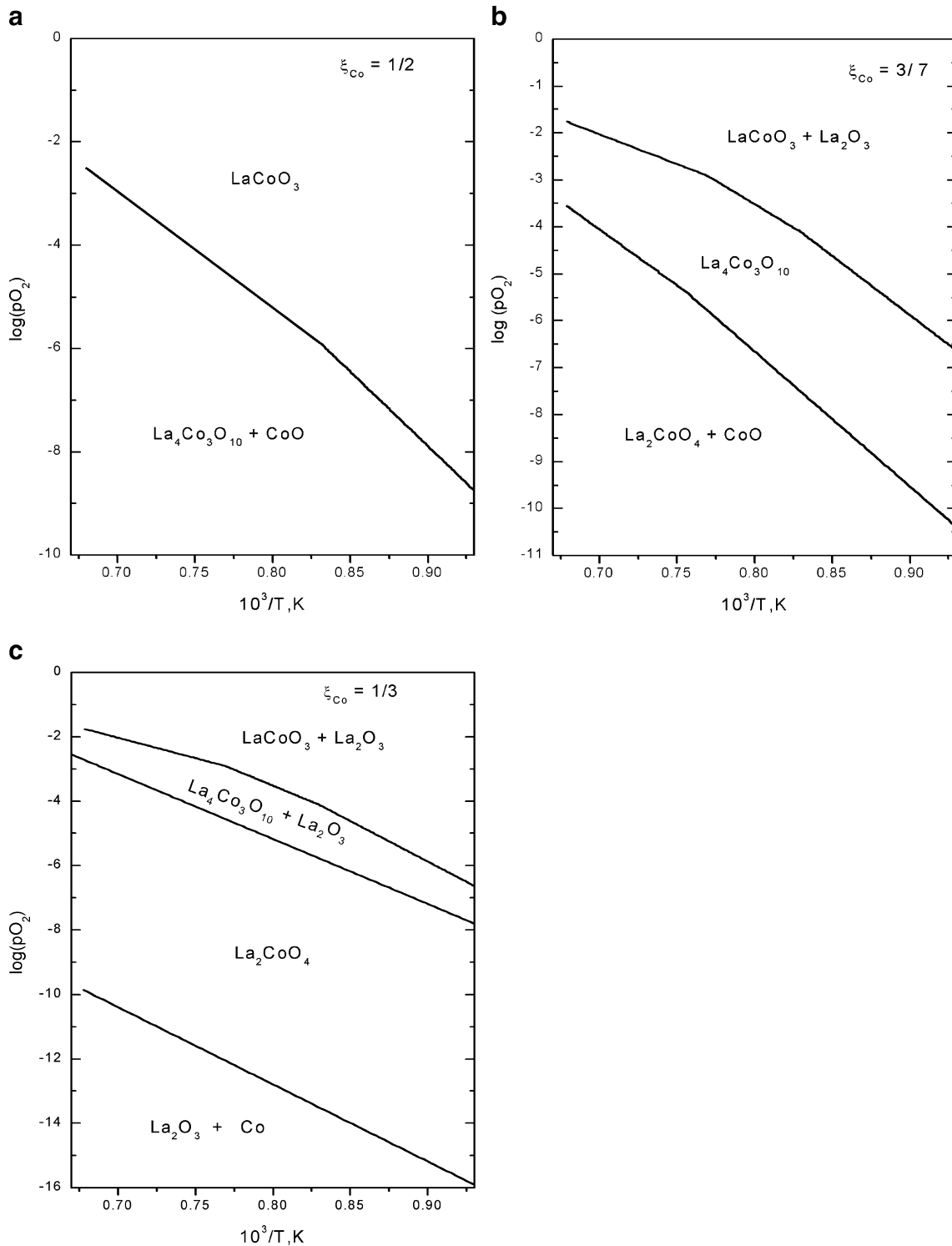


Fig. 3 Phase stability ranges for the ternary oxides in the La–Co–O system

stages of substitution, charge compensation occurs mostly by the increase of cobalt oxidation state (approximately up to $x \sim 0.3$) and at higher Me content by the increase of oxygen nonstoichiometry. The level of oxygen deficit is essentially independent of the nature of alkali earth metal (Fig. 4) [16, 17]. Nonetheless, as alkali earth metals (Ca, Sr,

Ba) have different polarization properties, the homogeneity ranges of $\text{La}_{1-x}\text{Me}_x\text{CoO}_{3-\delta}$ for Me=Ca, Sr, and Ba are substantially different. Phase equilibria in the La–Me–Co–O systems are shown in Figs. 5, 6, and 7.

Partial substitution of La^{3+} for Me^{2+} leads to decreasing thermodynamic stability of $\text{La}_{1-x}\text{Me}_x\text{CoO}_{3-\delta}$. The phase

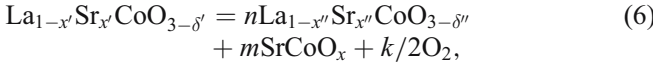
Table 1 Thermodynamic stability of LaTO_3 at 1,000 °C

Formula	$\log(\text{Po}_2)$	Measurement technique	Reference
LaMnO_3	-15.03	Gas chromatography	[6]
	-15.05	TGA	[7]
	-15.39	Conductivity measurements	[8]
	-14.9	TGA	[9]
LaFeO_3	-16.95	TGA	[7]
	-16.38	EMF	[10]
LaCoO_3	-5.5	EMF	[2]
	-4.78	EMF	[3, 4]
	-7.0	TGA	[7]
LaNiO_3	-0.6	TGA	[7]

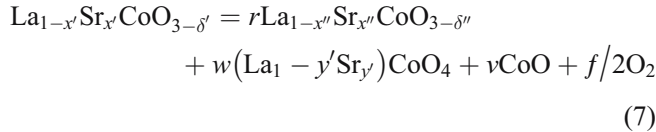
EMF electromotive force

equilibria in the $\text{La}-\text{Sr}-\text{Co}-\text{O}$ system along $(\text{La}+\text{Sr})$: $\text{Co}=1:1$ cross-section are shown in Fig. 8 [12, 13]. The mechanism of $\text{La}_{1-x}\text{Me}_x\text{CoO}_{3-\delta}$ decomposition on reduction changes and can be expressed by two reactions:

At 1,100 °C within $-0.68 \geq \log(\text{Po}_2) \geq -2.25$,



$$\begin{aligned} \text{where } & x' > x'', \quad n = (1 - x')/(1 - x''), \\ & m = (x' - x'')/(1 - x''), \\ & k = (3 - \delta') - (3 - \delta'') * n - x * m \end{aligned}$$



$$\begin{aligned} \text{where } & x' = r * x'' + 2w * y', \\ & r + w + v = 1 \\ & f = 3 - \delta' - r(3 - \delta'') - 4 * w - v \end{aligned}$$

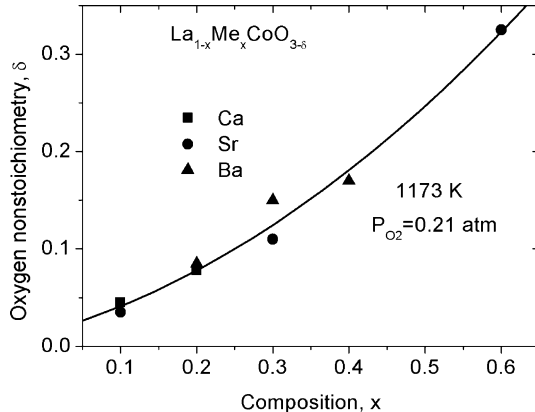


Fig. 4 The values of oxygen nonstoichiometry of $\text{La}_{1-x}\text{Me}_x\text{CoO}_{3-\delta}$ ($\text{Me}=\text{Ca}, \text{Sr}, \text{Ba}$) vs composition

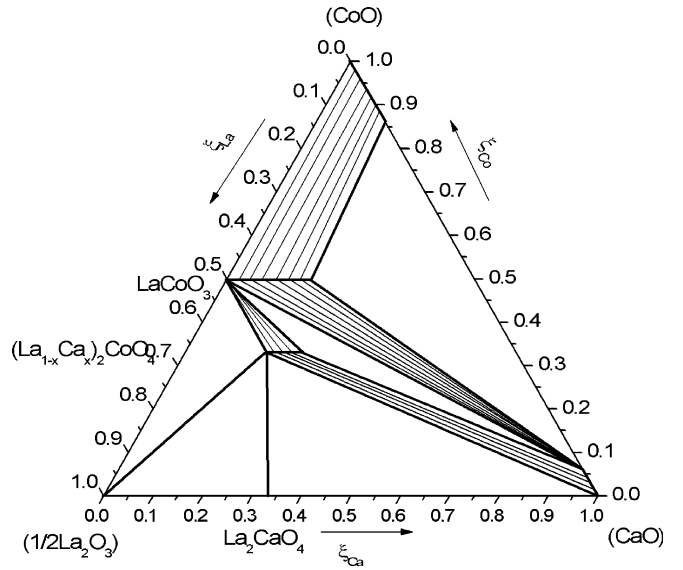


Fig. 5 Phase equilibria in the $\text{La}-\text{Ca}-\text{Co}-\text{O}$ system at 1,100 °C in air

La–Co–T–O systems (T=Mn, Fe, Ni, Cu)

The solid solutions in the $\text{La}-\text{Co}-\text{T}-\text{O}$ systems are based on the ternary oxides formed in the quasibinary $\text{La}-\text{T}-\text{O}$ systems. Two phases were described in the $\text{La}-\text{Mn}-\text{O}$ system, namely, $\text{LaMnO}_{3\pm\delta}$ (orthorhombically distorted perovskite, $Pbnm$ space group) stable in air and La_2MnO_4 in reduction atmospheres only at $T>1,380$ °C [6]. The only phase found in the $\text{La}-\text{Fe}-\text{O}$ system is LaFeO_3 (orthorhombically distorted perovskite, $Pbnm$ space group) [10]. The $\text{La}-\text{Ni}-\text{O}$ system comprises a maximum number of existing phases: La_2NiO_4 (with a tetragonal K_2NiF_4 -type structure, $I4/mmm$ space group), $\text{La}_3\text{Ni}_2\text{O}_7$ ($Cmcm$ space

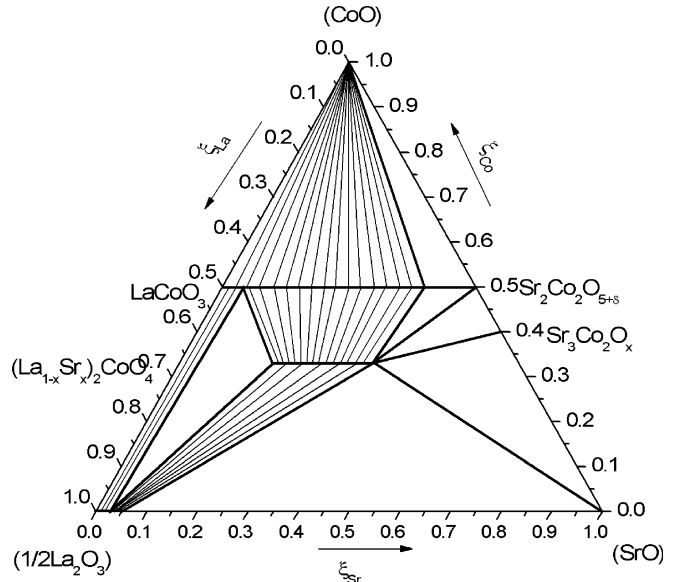


Fig. 6 Phase equilibria in the $\text{La}-\text{Sr}-\text{Co}-\text{O}$ system at 1,100 °C in air

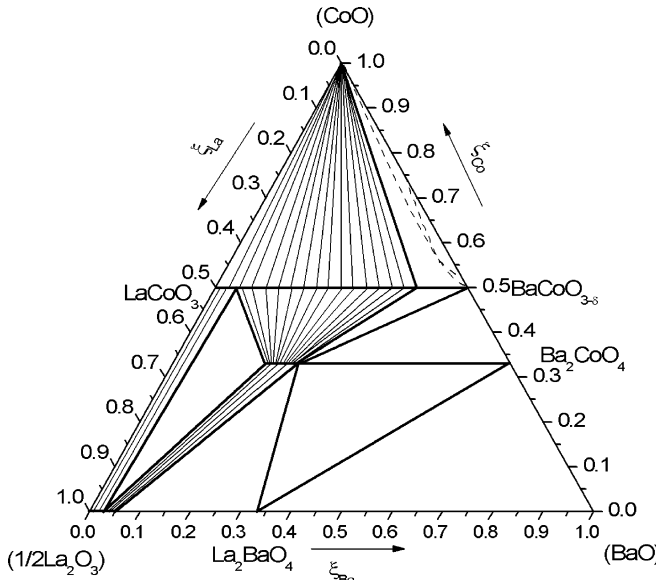


Fig. 7 Phase equilibria in the La–Ba–Co–O system at 1,100 °C in air

group), $\text{La}_4\text{Ni}_3\text{O}_{10}$ (*Cmca* space group), and $\text{LaNiO}_{3-\delta}$ (rhombohedrally distorted perovskite, $R\bar{3}c$ space group) [18–22]. In the La–Cu–O system, in addition to La_2CuO_4 [23], two other phases were found in narrow temperature ranges: $\text{La}_2\text{Cu}_2\text{O}_5$ (1,002–1,035 °C) and $\text{La}_8\text{Cu}_7\text{O}_{19}$ (1,012–1,027 °C) [24]. Another compound with perovskite-type structure, LaCuO_3 , was obtained at high oxygen pressure [25]. Depending on external conditions, $\text{LaCo}_{1-y}\text{T}_y\text{O}_3$ ($\text{T}=\text{Ni}, \text{Cu}$) solid solutions may exist either in the whole range or within a limited composition range [26–29]. For $\text{T}=\text{Fe}$ and Mn, a partial solubility takes place: from one side, based on LaCoO_3 ($R\bar{3}c$) and from another

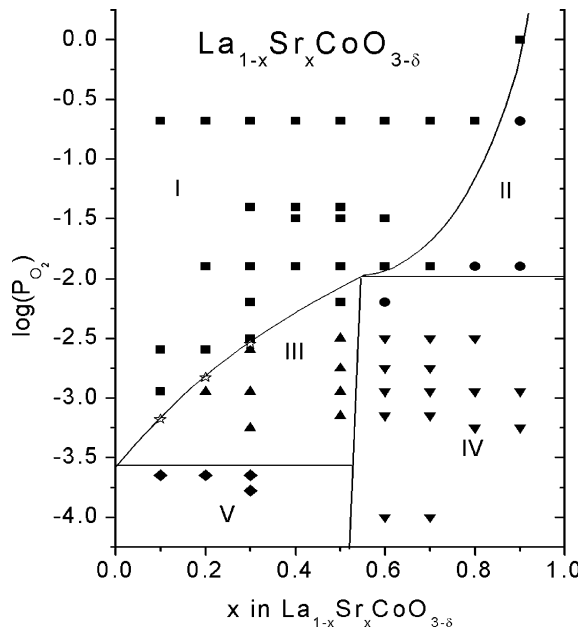


Fig. 8 The cross-sections of the La–Sr–Co–O phase diagram along $\text{La}_{1-x}\text{Sr}_x\text{CoO}_{3-\delta}$

side, with the *Pbnm* space group [30–32]. Phase equilibria in some La–Co–T–O systems are shown in Figs. 9, 10, and 11.

Quaternary systems

Oxide materials based on lanthanum cobaltite with simultaneous partial substitution of La for alkali earth elements and Co for other 3d-transition metals, such as $\text{La}_{1-x}\text{Me}_x\text{Co}_{1-y}\text{T}_y\text{O}_{3-\delta}$ or $(\text{La}_{1-x}\text{Me}_x)_2\text{Co}_{1-y}\text{T}_y\text{O}_{4\pm\delta}$, belong to the corresponding quaternary systems.

Phase equilibria in La–Sr(Ba)–Co–Mn–O systems are shown in Figs. 12 and 13 [33, 34]. The structure and homogeneity range of $\text{La}_{1-x}\text{Me}_x\text{Co}_{1-y}\text{Mn}_y\text{O}_{3\pm\delta}$ ($\text{Me}=\text{Sr}, \text{Ba}$) depend significantly on the values of x and y . The perovskites $\text{La}_{0.95}\text{Me}_{0.05}\text{Co}_{1-y}\text{Mn}_y\text{O}_{3\pm\delta}$ ($0\leq y\leq 0.5$ for $\text{Me}=\text{Sr}$; $0\leq y\leq 0.4$ for $\text{Me}=\text{Ba}$) and $\text{La}_{0.9}\text{Me}_{0.1}\text{Co}_{1-y}\text{Mn}_y\text{O}_{3\pm\delta}$ ($0\leq y\leq 0.7$ for $\text{Me}=\text{Sr}$, and $0\leq y\leq 0.4$ for $\text{Me}=\text{Ba}$) have a rhombohedrally distorted lattice similar to LaCoO_3 . For $\text{La}_{0.95}\text{Me}_{0.05}\text{Co}_{1-y}\text{Mn}_y\text{O}_{3\pm\delta}$ ($0.8\leq y\leq 1$ for $\text{Me}=\text{Sr}$; $0.7\leq y\leq 1$ for $\text{Me}=\text{Ba}$) and $\text{La}_{0.9}\text{Me}_{0.1}\text{Co}_{1-y}\text{Mn}_y\text{O}_{3\pm\delta}$ ($0.9\leq y\leq 1$ for $\text{Me}=\text{Sr}$, $0.8\leq y\leq 1$ for $\text{Me}=\text{Ba}$), an orthorhombic structure similar to $\text{LaMnO}_{3\pm\delta}$ (S.G. *Pnma*) is formed. Two-phase regions, where rhombohedral and orthorhombic phases coexist, were found at $0.5\leq y\leq 0.8$ ($\text{Me}=\text{Sr}$) and at $0.4\leq y\leq 0.7$ ($\text{Me}=\text{Ba}$) for $x=0.05$, and $0.7\leq y\leq 0.9$ ($\text{Me}=\text{Sr}$) and $0.4\leq y\leq 0.8$ ($\text{Me}=\text{Ba}$) for $x=0.1$. The crystal structure of $\text{La}_{1-x}\text{Me}_x\text{Co}_{1-y}\text{Mn}_y\text{O}_{3\pm\delta}$ for $x=0.2$ ($\text{Me}=\text{Sr}, \text{Ba}$) and 0.3 ($\text{Me}=\text{Sr}$) was found to be rhombohedral for all values of y , in agreement with the shift of orthorhombic \leftrightarrow rhombohedral transition in $\text{La}_{1-x}\text{Me}_x\text{MnO}_{3\pm\delta}$ at 1,100 °C [35]. The compositions in the vicinity of $\text{La}_{1-x}\text{Me}_x\text{CoO}_{3-\delta}$ ($0.5\leq x\leq 0.8$) are cubic, space group *Pm3m*. The fields I and III show the solid solutions of general formula $\text{La}_{1-x}\text{Sr}_x\text{Co}_{1-y}\text{Mn}_y\text{O}_{3\pm\delta}$ with orthorhombic (I), rhombohedral (III) or cubic (IIIa) structures, respectively.

The solubility of nickel in perovskite-type $\text{La}_{1-x}\text{Sr}_x\text{Co}_{1-y}\text{Ni}_y\text{O}_{3\pm\delta}$ decreases when strontium content increases.

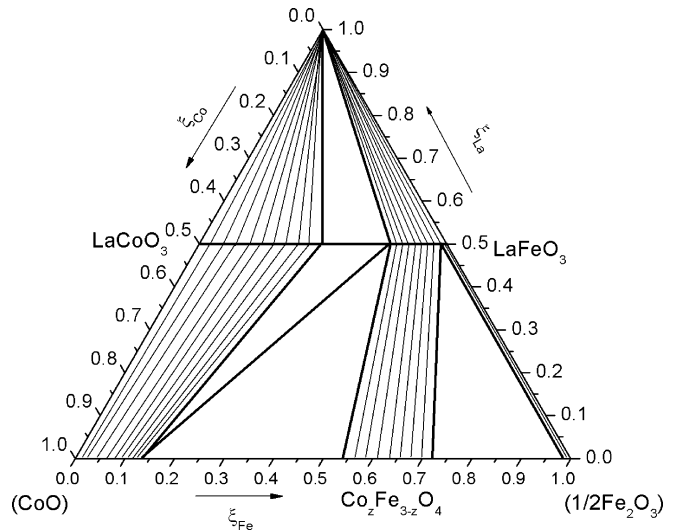


Fig. 9 Phase equilibria in the La–Co–Fe–O system at 1,100 °C in air

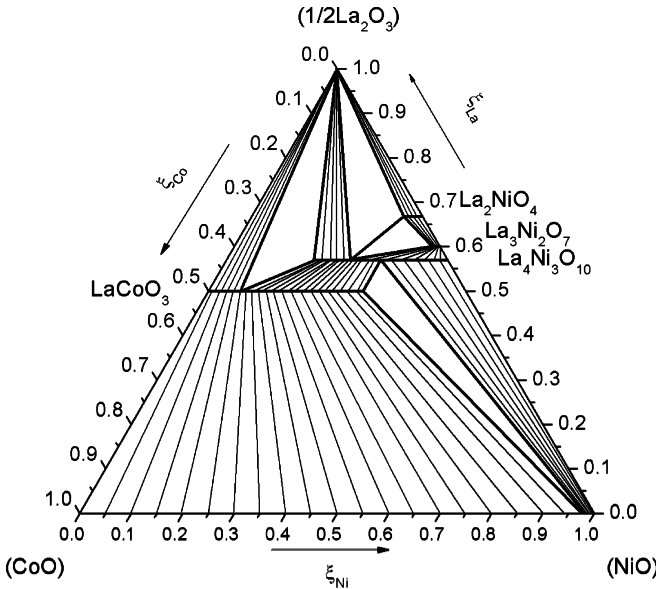


Fig. 10 Phase equilibria in the La–Co–Ni–O system at 1,100 °C in air

This is in a good agreement with the fact that strontium substitution, in general, increases the average oxidation state of 3d-transition metal, while nickel substitution leads to the opposite effect. The field of phase stability is shown in Fig. 14. As for lanthanum strontium cobaltites, the rhombohedral distortions of $\text{La}_{1-x}\text{Sr}_x\text{Co}_{1-y}\text{Ni}_y\text{O}_{3-\delta}$ decrease when Sr content increases. For example, $\text{La}_{0.5}\text{Sr}_{0.5}\text{Co}_{0.9}\text{Ni}_{0.1}\text{O}_{3-\delta}$ still has a small rhombohedral distortion, whereas lanthanum–strontium cobaltite is already cubic at $x=0.5$ [36].

For $(\text{La}_{1-x}\text{Sr}_x)_2\text{Co}_{1-y}\text{Ni}_y\text{O}_{4\pm\delta}$ system, the phase boundaries are essentially linear, Fig. 15 [37]. These are in a good agreement with the homogeneity ranges of $(\text{La}_{1-x}\text{Sr}_x)_2\text{CoO}_{4\pm\delta}$ [12, 13], $(\text{La}_{1-x}\text{Sr}_x)_2\text{NiO}_{4\pm\delta}$ [38] and $\text{La}_2\text{Co}_{1-y}\text{Ni}_y\text{O}_{4\pm\delta}$ [26]. All $(\text{La}_{1-x}\text{Sr}_x)_2\text{Co}_{1-y}\text{Ni}_y\text{O}_{4\pm\delta}$

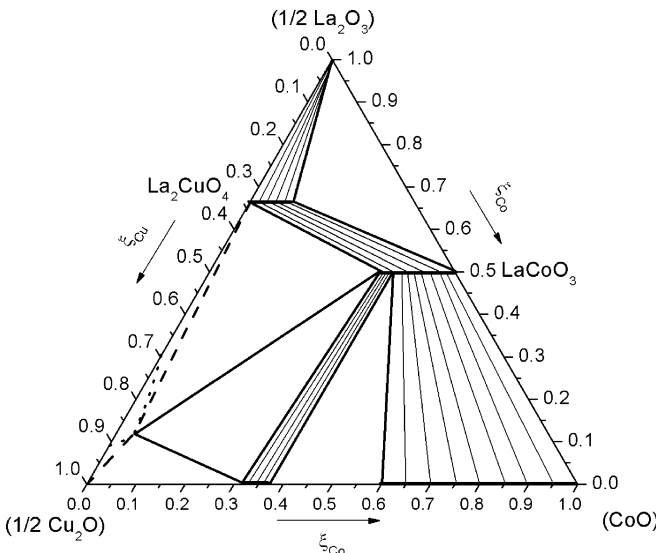


Fig. 11 Phase equilibria in the La–Co–Cu–O system at 1,100 °C in air

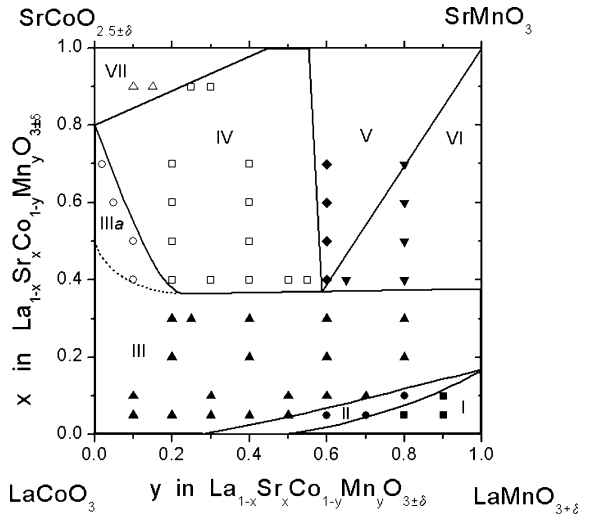


Fig. 12 The phase equilibria of the $\text{LaCoO}_3 - \text{LaMnO}_{3+\delta} - \text{SrCoO}_{2.5\pm\delta} - \text{SrMnO}_3$ system at 1,100 °C in air

solid solutions have tetragonal K_2NiF_4 type structure (space group $I4/mmm$).

Defect chemistry

The substitution of Sr for lanthanum increases both the electronic and oxide ion conductivity of lanthanum cobaltite by introducing holes and oxygen vacancies, respectively [39]. Doping with a transition metal such as Cu leads to increasing oxygen nonstoichiometry and a substantial improvement of electrocatalytic activity of cathodes based on LaCoO_3 [40, 41]. The key properties of doped lanthanum cobaltites, such as oxide-ion and total electrical conductivities, are directly related to their defect structure. The Sr-doped lanthanum cobaltite received much

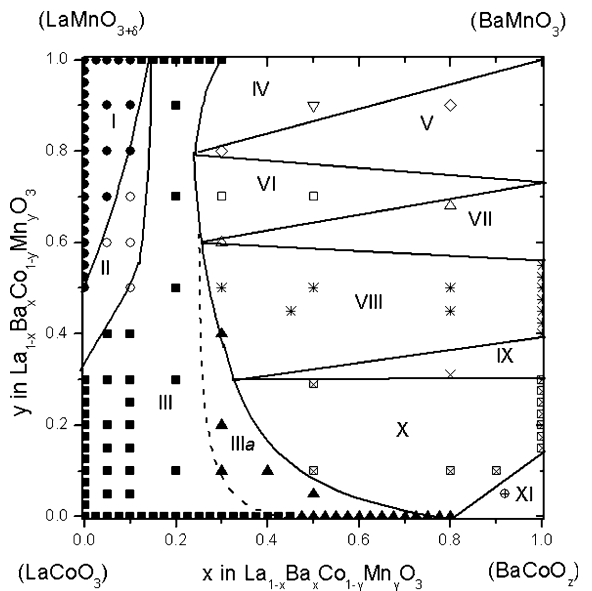


Fig. 13 The phase equilibria of the $\text{LaCoO}_3 - \text{LaMnO}_{3+\delta} - \text{BaCoO}_2 - \text{BaMnO}_3$ system at 1,100 °C in air

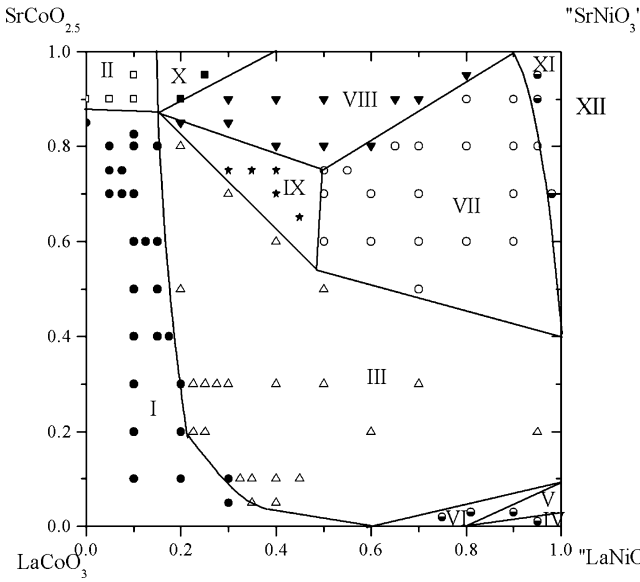


Fig. 14 The phase equilibria of the LaCoO_3 – LaNiO_3 – SrCoO_2 – SrNiO_3 system at 1,100 °C in air

attention in this respect. The oxygen nonstoichiometry and the defect structure of $\text{La}_{1-x}\text{Sr}_x\text{CoO}_{3-\delta}$ were studied by Mizusaki et al. [42, 43], Petrov et al. [44, 45], Lankhorst et al. [46–48], and Kozhevnikov et al. [49, 50]. Lankhorst et al. [46–48] described the defect structure of $\text{La}_{1-x}\text{Sr}_x\text{CoO}_{3-\delta}$ ($x=0.2, 0.4, 0.7$) in the framework of the electron gas rigid band model, assuming that electrons created during vacancy formation are placed in broad electron band [47]. Contrary to the conclusions of Lankhorst et al. [46–48], $\text{La}_{1-x}\text{Sr}_x\text{CoO}_{3-\delta}$ ($x=0.3, 0.6$) was found to be a typical narrow-band conductor at elevated temperatures [49, 50]. Mizusaki et al. [43] emphasized that $\text{La}_{1-x}\text{Sr}_x\text{CoO}_{3-\delta}$ is not a wide-band gap semiconductor because there is no plateau on p_{O_2} dependencies of its oxygen

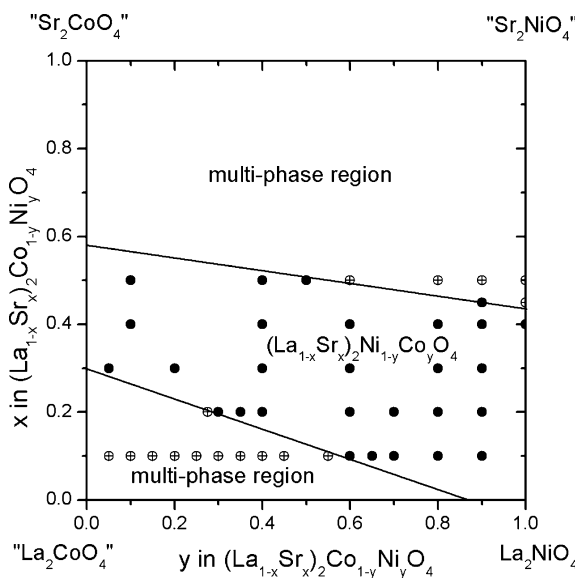


Fig. 15 The homogeneity range of the $(\text{La}_{1-x}\text{Sr}_x)_2\text{Co}_{1-y}\text{Ni}_y\text{O}_{4\pm\delta}$ solid solution at 1,100 °C in air

nonstoichiometry at $\delta=x/2$. Therefore, the electrons are not strongly localized on Co ions.

The oxygen nonstoichiometry of Cu-doped lanthanum cobaltite was measured and some preliminary results on the defect structure were reported by us earlier [40, 51, 52]. For undoped LaCoO_3 , the nonstoichiometry was studied only in a few works. First, Seppanen et al. [53] measured δ as a function of p_{O_2} using the coulometric titration technique at 900–1,038 °C; randomly distributed oxygen vacancies with different charges were assumed to be the anionic defects in LaCoO_3 . Later, Petrov et al. [54] studied the oxygen nonstoichiometry of $\text{LaCoO}_{3-\delta}$ as a function of p_{O_2} using the TGA method in high temperature range $1,000 \leq T, ^\circ\text{C} \leq 1,400$. The oxygen nonstoichiometry of $\text{LaCoO}_{3-\delta}$ was also studied by Mizusaki et al. [43] on a single crystal sample at the temperatures between 900 and 1,000 °C. The defect structure of this oxide was discussed in terms of partial molar enthalpy and entropy of oxygen. It is necessary to note that the values of oxygen nonstoichiometry of $\text{LaCoO}_{3-\delta}$ reported by Mizusaki et al. [43] are higher than those measured by Seppanen et al. [53] by about an order of magnitude at low p_{O_2} and the same temperature. To date, there are no data concerning the quantitative modeling of the defect structure of undoped lanthanum cobaltite. Recently, Zuev et al. (submitted for publication) measured the oxygen nonstoichiometry of undoped lanthanum cobaltite as a function of oxygen partial pressure and in the temperature range between 1,173 and 1,323 K by use of coulometric titration technique. Their results were coincident with those obtained by Seppanen et al. [53]. Thus, the defect structure of undoped and doped lanthanum cobaltites is still a subject of debate.

Models of the defect structure of undoped and Sr-doped LaCoO_3

Because the oxygen nonstoichiometry of lanthanum cobaltite seems to have relatively low values, let us only consider the randomly distributed point defects and assume also that Sr as A-site dopant traps electrons ($\text{Sr}_{\text{La}}^{\text{I}}$ using Kröger–Vink notation). Strontium is believed to remain divalent irrespective of p_{O_2} and temperature. The concentration of $\text{Sr}_{\text{La}}^{\text{I}}$ may be, therefore, simply replaced by total concentration of the dopant x . Moreover, it is not clear so far whether electrons which are not trapped on Sr sites and holes are delocalized or localized on cobalt sites. Two different models should be, therefore, analyzed.

Within the framework of *model 1*, the approach of itinerant electronic species is accepted, then the condition of charge neutrality is given as:

$$p + 2[V_O^{\bullet\bullet}] = n + x. \quad (8)$$

If electrons and holes localized on Co sites (*model 2*),

$$[Co_{\text{Co}}^{\bullet}] + 2[V_O^{\bullet\bullet}] = [Co_{\text{Co}}^{\text{I}}] + x, \quad (8\text{a})$$

where the Kröger–Vink notation is used. Intrinsic disordering with equilibrium constant

$$nil = e^{\prime} + h^{\bullet},$$

with equilibrium constant

$$K_9 = np \quad (10)$$

should be taken into account for *model 1*. The reaction of charge disproportionation involving the transfer of an electron between adjacent Co_{Co}^{\times} sites



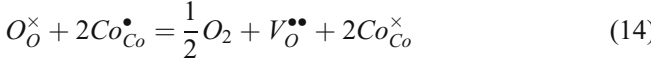
with equilibrium constant

$$K_{11} = \frac{[Co_{Co}^{\prime}][Co_{Co}^{\bullet}]}{[Co_{Co}^{\times}]^2} \quad (12)$$

should be, accordingly, considered in *model 2*. Furthermore, the process of oxygen release from the cobalt lattice under reducing conditions is accompanied by the holes' consumption (*model 1*)



or by the reduction of Co^{4+} to Co^{3+} according to *model 2*

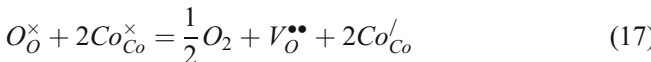


The equilibrium constants of the reactions Eqs. 13 and 14 can be given as

$$K_{13} = \frac{[V_O^{\bullet\bullet}]p_{O2}^{0.5}}{[O_O^{\times}]p^2} \quad (15)$$

$$K_{14} = \frac{[V_O^{\bullet\bullet}][Co_{Co}^{\times}]^2 p_{O2}^{0.5}}{[O_O^{\times}][Co_{Co}^{\bullet}]^2} \quad (16)$$

The combination of the aforementioned reactions allows deriving other defect reactions. The subtraction of Eq. 11 from Eq. 14, for instance, yields the following reaction of the defect formation:



$$K_{17} = \frac{[V_O^{\bullet\bullet}][Co_{Co}^{\prime}]^2 p_{O2}^{0.5}}{[O_O^{\times}][Co_{Co}^{\times}]^2} \quad (18)$$

It is evident that only two reactions from Eqs. 11, 14, and 17 are independent of each other and, therefore, may be used for modeling.

Considering the mass balance condition and the obvious definition $[V_O^{\bullet\bullet}] = \delta$, the following sets of nonlinear equations can be given for these models:

– Model 1:

$$\begin{cases} K_9 = np = K_9^o \exp\left(-\frac{\Delta H_9^o}{RT}\right) \\ K_{13} = \frac{\delta p_{O2}^{0.5}}{(3-\delta)p^2} = K_{13}^o \exp\left(-\frac{\Delta H_{13}^o}{RT}\right) \\ p + 2\delta = n + x \end{cases} \quad (19)$$

The analytical solutions include

$$p = \frac{x}{2} + \frac{\sqrt{4\delta^2 - 4\delta x + x^2 + 4K_9}}{2} - \delta = f_h(T, \delta) \quad (20)$$

and

$$\log(p_{O2}/atm) = 4 \log\left(\frac{\sqrt{K_{13}}\sqrt{3-\delta}(2\delta-x-\sqrt{4\delta^2-4\delta x+x^2+4K_9})}{-2\sqrt{\delta}}\right) \quad (21)$$

– Model 2:

$$\begin{cases} K_{11} = \frac{[Co_{Co}^{\prime}][Co_{Co}^{\bullet}]}{[Co_{Co}^{\times}]^2} = K_{11}^o \exp\left(-\frac{\Delta H_{11}^o}{RT}\right) \\ K_{17} = \frac{\delta [Co_{Co}^{\prime}]^2 p_{O2}^{0.5}}{(3-\delta)[Co_{Co}^{\times}]^2} = K_{17}^o \exp\left(-\frac{\Delta H_{17}^o}{RT}\right). \\ [Co_{Co}^{\bullet}] + 2\delta = [Co_{Co}^{\prime}] + x \\ [Co_{Co}^{\bullet}] + [Co_{Co}^{\prime}] + [Co_{Co}^{\times}] = 1 \end{cases} \quad (22)$$

The analytical solutions of this set with physical meaning are the concentrations of localized electrons

$$\begin{aligned} [Co'_{Co}] &= \frac{4K_{11} - 4K_{11}x + x + 8K_{11}\delta - 2\delta +}{2(4K_{11} - 1)} \\ &= f'_h(T, \delta) \end{aligned} \quad (23)$$

and

$$\log(p_{O_2}/atm) = 4\log \left\{ \frac{2\sqrt{K_{10}}\sqrt{(3-\delta)(-1-C)}}{(4K_{11}-4K_{11}x+x+8K_{11}\delta-2\delta+C)\cdot\sqrt{\delta}} \right\}, \quad (24)$$

where

$$C = -\sqrt{4K_{11} + 4\delta^2 - 4x\delta + x^2 - 4K_{11}x^2 - 16K_{11}\delta^2 + 16K_{11}\delta^2}.$$

The Eqs. 21 and 24 can then be used for fitting of the experimental data on the oxygen nonstoichiometry of $\text{LaCoO}_{3-\delta}$.

Models of the defect structure of Cu-doped lanthanum cobaltite

Partial replacement of cobalt by copper causes a substantial increase of oxygen deficiency in $\text{LaCo}_{1-x}\text{Cu}_x\text{O}_{3-\delta}$ [51, 52]. Copper introduced into the cobalt sublattice becomes an electron acceptor (Cu'_{Co}), as copper is more electronegative compared to cobalt. The negative charge excess of acceptor defects in the oxide structure is balanced by the corresponding amount of positive charges, oxygen vacancies, and/or electron holes. The formation of equilibrium electronic point defects can be described again within the framework of either quasi-free (h^\bullet) or localized-electrons (Co^\bullet_{Co}) models. Then, the charge neutrality condition in the case of the itinerant nature of electrons and holes in the Cu-doped lanthanum cobaltite (*model 1A*) is given as

$$p + 2[V_O^{\bullet\bullet}] = n + [Cu'_{Co}] \quad (25)$$

For localized electronic species in $\text{LaCo}_{1-x}\text{Cu}_x\text{O}_{3-\delta}$ (*model 2A*), the charge neutrality condition requires that

$$[Co^\bullet_{Co}] + 2[V_O^{\bullet\bullet}] = [Cu'_{Co}] + [Co'_{Co}] \quad (26)$$

Copper may change its oxidation state depending on p_{O_2} and temperature, contrary to Sr. The concentration of Cu'_{Co} cannot, therefore, be simply replaced by total concentration of the dopant x in Eqs. 25 and 26 and the following reactions

$$Cu_{Cu}^\times = Cu'_{Co} + h^\bullet \quad (27)$$

with the equilibrium constant

$$K_{27} = \frac{[Cu'_{Co}]p}{[Cu_{Co}^\times]} \quad (28)$$

and

$$Cu_{Co}^\times + Co_{Co}^\times = Cu'_{Co} + Co_{Co}^\bullet \quad (29)$$

with the equilibrium constant

$$K_{29} = \frac{[Cu'_{Co}][Co_{Co}^\bullet]}{[Cu_{Co}^\times][Co_{Co}^\times]} \quad (30)$$

should be taken into account in *Models 1A* and *2A*, respectively. Solving Eqs. 13 and 27 or Eqs. 14 and 29 gives the reaction of oxygen incorporation

$$O_O^\times + 2Cu_{Co}^\times = \frac{1}{2}O_2 + V_O^{\bullet\bullet} + 2Cu'_{Co}, \quad (31)$$

the equilibrium constants of which is

$$K_{31} = \frac{[V_O^{\bullet\bullet}][Cu'_{Co}]^2 p_{O2}^{0.5}}{[O_O^\times][Cu_{Co}^\times]^2}. \quad (32)$$

The reactions Eqs. 9, 27, and 31, or Eqs. 11, 29, and 31, are independent and, therefore, can be used for modeling. The resultant sets of nonlinear equations include:

– Model 1A

$$\begin{cases} K_9 = np = K_9^o \exp \left(-\frac{\Delta H_9^o}{RT} \right) \\ K_{27} = \frac{[Cu'_{Co}]p}{[Cu_{Co}^\times]} = K_{27}^o \exp \left(-\frac{\Delta H_{27}^o}{RT} \right) \\ K_{31} = \frac{[V_O^{\bullet\bullet}][Cu'_{Co}]^2 p_{O2}^{0.5}}{[O_O^\times][Cu_{Co}^\times]^2} = K_{31}^o \exp \left(-\frac{\Delta H_{31}^o}{RT} \right) \\ p + 2\delta = n + [Cu'_{Co}] \\ [Cu'_{Co}] + [Cu_{Co}^\times] = x \end{cases} \quad (33)$$

These combined equations can be solved analytically. Then, a cubic equation with respect to the concentration of quasi-free holes can be derived:

$$ap^3 + bp^2 + cp - d = 0 \quad (34)$$

The analytical solution of this equation, with physical meaning, is the concentration of itinerant holes

$$p = \frac{B^{1/3}}{6} - \frac{6\left(\frac{c}{3} - \frac{b^2}{9}\right)}{B^{1/3}} - \frac{b}{3} = f_h(T, \delta), \quad (35)$$

where $a = 1$, $b = (2\delta + K_{27})$, $c = (-K_{27}x + 2\delta K_{27} - K_9)$, $d = K_9 K_{27}$ and $B = 36cb - 108d - 8b^3 + 12\sqrt{12c^3 - 3c^2b^2 - 54cbd + 81d^2 + 12db^3}$.

The substitution of Eq. 35 in Eq. 32 using the charge neutrality and mass balance conditions yields a necessary model equation

$$\log(p_{O_2}/atm) = 4 \log \left(\frac{K_{31}^{0.5}(3-\delta)^{0.5}(x - \frac{K_{27}x}{D})D}{K_{27}x\delta^{0.5}} \right), \quad (36)$$

where $D = K_{27} + \frac{B}{6} - \frac{2(3c - b^2)}{3B} - \frac{b}{3}$.

- Model 2A

The set of nonlinear equations now consists of expressions for equilibrium constant Eqs. 12, 30, and 32, and chargeneutrality condition Eq. 26, along with mass balance conditions $[Cu_{Co}^\times] + [Cu_{Co}'] = x$ and $[Co_{Co}^\times] + [Co_{Co}^\bullet] + [Co_{Co}'] = 1 - x$. Appropriate substitutions lead to the cubic equation with respect to the concentration of divalent copper Cu_{Co}'

$$a[Cu_{Co}']^3 + b[Cu_{Co}']^2 + c[Cu_{Co}'] + d = 0, \quad (37)$$

where $a = K_{11} + K_{29}^2 - K_{29}$, $b = K_{11}(1 - x - 2\delta) + K_{29}(x - K_{11}x - K_{11} - 2K_{11}\delta + 2\delta)$ and $c = K_{11}(2K_{11}x - K_{11}x^2 + 4K_{11}\delta x - 2\delta x)$, $d = K_{11}(-K_{11}x^2 + K_{11}x^3 - 2K_{11}\delta x^2)$. The solution is given as

$$[Cu_{Co}'] = \frac{B^{1/3}}{6} - \frac{6\left(\frac{c}{3} - \frac{b^2}{9}\right)}{B^{1/3}} - \frac{b}{3} = f_{Cu_{Co}'}(T, \delta). \quad (38)$$

The latter allows us to express p_{O_2} explicitly from Eq. 31 as a function of oxygen nonstoichiometry to verify whether model 2A fits the experimental data. This expression is similar to that discussed for the previous model, and therefore, it was omitted here.

Models of the defect structure of Sr- and Mn-doped lanthanum cobaltite

The partial replacement of cobalt by manganese causes a substantial decrease of oxygen deficiency in the $\text{La}_{1-x}\text{Sr}_x$

$\text{Co}_{1-z}\text{Mn}_z\text{O}_{3-\delta}$ oxides [50], suggesting a donor-type behavior of manganese cations (Mn_{Co}^\bullet). The positive charge excess of the donor defects in the oxide structure is balanced now by the corresponding amount of negative charges, namely, electrons. The defect chemistry can be described, again, by models assuming either quasi-free electrons (e') or localized electrons (Co_{Co}'). For the itinerant model (model 1B), the electroneutrality and charge disproportionation conditions give

$$[Mn_{Co}^\bullet] + p + 2[V_O^{\bullet\bullet}] = n + x \quad (39)$$

For localized electrons in $\text{La}_{1-x}\text{Sr}_x\text{Co}_{1-z}\text{Mn}_z\text{O}_{3-\delta}$ (model 2B),

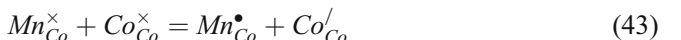
$$[Co_{Co}^\bullet] + [Mn_{Co}^\bullet] + 2[V_O^{\bullet\bullet}] = x + [Co_{Co}'] \quad (40)$$

To account for the changes in manganese oxidation state, the following reactions



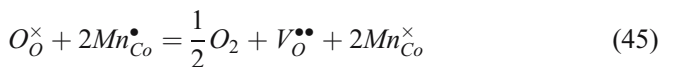
$$K_{41} = \frac{[Mn_{Co}^\bullet]n}{[Mn_{Co}^\times]} \quad (42)$$

and



$$K_{43} = \frac{[Mn_{Co}^\bullet][Co_{Co}']}{[Mn_{Co}^\times][Co_{Co}^\times]} \quad (44)$$

should be considered for Models 1B and 2B, respectively. Let us assume further that the defect reactions Eqs. 9 and 13, or Eqs. 11 and 14, are valid for $\text{La}_{1-x}\text{Sr}_x\text{Co}_{1-z}\text{Mn}_z\text{O}_{3-\delta}$ depending on the model as well. These result in



$$K_{45} = \frac{[V_O^{\bullet\bullet}][Mn_{Co}^\times]^2 p_{O_2}^{0.5}}{[O_O^\times][Mn_{Co}^\bullet]^2}. \quad (46)$$

The final sets of equations become:

– Model 1B:

$$\left\{ \begin{array}{l} K_9 = np = K_9^o \exp \left(-\frac{\Delta H_9^o}{RT} \right) \\ K_{13} = \frac{\delta p_{O_2}^{0.5}}{(3-\delta)p^2} = K_{13}^o \exp \left(-\frac{\Delta H_{13}^o}{RT} \right) \\ K_{41} = \frac{[Mn_{Co}^\bullet]n}{[Mn_{Co}^\times]} = K_{41}^o \exp \left(-\frac{\Delta H_{41}^o}{RT} \right) \\ [Mn_{Co}^\bullet] + p + 2[V_O^{\bullet\bullet}] = n + x \\ [Mn_{Co}^\times] + [Mn_{Co}^\bullet] = z \end{array} \right. \quad (47)$$

Solving the cubic equation with respect to the concentration of quasi-free electrons

$$an^3 + bn^2 + cn + d = 0, \quad (48)$$

one can obtain the analytical solution for the concentration of itinerant electrons

$$n = \frac{B^{1/3}}{6} - \frac{6\left(\frac{c}{3} - \frac{b^2}{9}\right)}{B^{1/3}} - \frac{b}{3} = f_n(T, \delta), \quad (49)$$

where $a = -1$, $b = -K_{41} + 2\delta - x$, $c = K_9 + 2\delta K_{41} - xK_{41} + zK_{41}$, $d = K_9 K_{41}$ and $B = 36cb - 108d - 8b^3 + 12\sqrt{12c^3 - 3c^2b^2 - 54cbd + 81d^2 + 12db^3}$.

The substitution of Eq. 49 in Eq. 13 using Eq. 9 yields a necessary model equation.

– Model 2B:

The set of nonlinear equations now consists of expressions for equilibrium constant Eqs. 12, 44, and 46; the charge neutrality condition Eq. 40; and the mass balance conditions $[Mn_{Co}^\times] + [Mn_{Co}^\bullet] = z$, and $[Co_{Co}^\times] + [Co_{Co}^\bullet] + [Co_{Co}'^\bullet] = 1 - z$. Appropriate substitutions lead to the cubic equation with respect to Mn_{Co}^\bullet

$$a[Mn_{Co}^\bullet]^3 + b[Mn_{Co}^\bullet]^2 + c[Mn_{Co}^\bullet] + d = 0, \quad (50)$$

where $a = K_{11} + K_{43}^2 - K_{43}$, $b = K_{11}(1 - z + 2\delta - x) + K_{43}(2K_{43}\delta + z - K_{43}x - K_{43}z + x - K_{43} - 2\delta)$, and $c = K_{43}(2K_{43}z - zx + 2K_{43}zx + 2z\delta - K_{43}z^2 - 4K_{43}z\delta)$, $d = K_{43}(2K_{43}z^2\delta - K_{43}z^2 + K_{43}z^3 - K_{43}z^2x)$. The solution of the cubic equation with a physical meaning makes it possible to express p_{O_2} explicitly from Eq. 11 as a function of oxygen nonstoichiometry to verify model2B by the experimental data.

Discussion

Because the changes in oxygen stoichiometry of perovskite-type $\text{La}_{1-x}\text{Sr}_x\text{CoO}_{3-\delta}$ ($x=0, 0.3, 0.6$), $\text{La}_{0.7}\text{Sr}_{0.3}\text{Co}_{0.75}\text{Mn}_{0.25}\text{O}_{3-\delta}$, and $\text{LaCo}_{0.7}\text{Cu}_{0.3}\text{O}_{3-\delta}$ were measured in a relatively narrow temperature range, the defect formation enthalpies can be assumed to be constant over the whole temperature range investigated. This assumption makes it possible to substitute equilibrium constants by their temperature dependencies [e.g., Eqs. 19, 22, and 33] and to treat the data on oxygen nonstoichiometry obtained at different temperatures simultaneously. As an example, the fitting results for $\text{LaCoO}_{3-\delta}$ using *model 1* described by Eq. 21 and *model 2* described by Eq. 24 are shown in Fig. 16a,b. It is evident that there is good agreement between the experimental data and the fitting results for both *model 1* and *model 2*. The correlation coefficient R^2 is virtually indistinguishable for the two models (Table 2). The data on other compounds (Table 2) lead to similar conclusions. Therefore, the question if electron holes are localized cannot be solved solely on the basis of the data on oxygen nonstoichiometry.

The equilibrium constants of defect reactions obtained in this work by fitting allow us to calculate the isothermal dependencies of point defect concentrations on oxygen nonstoichiometry or oxygen partial pressure. Such dependencies are shown in Figs. 17, 18, 19, and 20 for $\text{LaCoO}_{3-\delta}$, $\text{La}_{0.7}\text{Sr}_{0.3}\text{CoO}_{3-\delta}$ and $\text{La}_{0.7}\text{Sr}_{0.3}\text{Co}_{0.75}\text{Mn}_{0.25}\text{O}_{3-\delta}$, $\text{La}_{0.4}\text{Sr}_{0.6}\text{CoO}_{3-\delta}$, and $\text{LaCo}_{0.7}\text{Cu}_{0.3}\text{O}_{3-\delta}$, respectively, at 900°C. As can be seen, the trends in change of the concentrations of electrons and holes with oxygen nonstoichiometry are similar, irrespective of the nature of electronic defects. The second conclusion is that the hole concentration in Cu-doped cobaltite is lower than that in $\text{La}_{0.7}\text{Sr}_{0.3}\text{CoO}_{3-\delta}$ by about a factor of 5. This obviously indicates that formation of negative-charged defects Cu_{Co}^- is accompanied by the oxygen vacancy formation according to reaction Eq. 31, rather than hole generation. A similar trend was recently reported for $\text{LaCr}_{0.79}\text{Cu}_{0.05}\text{Al}_{0.16}\text{O}_{3-\delta}$ with the same crystal structure [55]. The addition of copper in chromite was found to result in the oxygen vacancy formation and did not change the chromium oxidation state (3+). In contrast, copper changes the oxidation state continuously from 3+ via 2+ to 1+ when the oxygen partial pressure decreases.

Charge transfer

The Sr (Ca or Ba)-doped lanthanum cobaltites $\text{La}_{1-x}\text{A}_x\text{CoO}_{3-\delta}$ are mixed conductors with high oxygen-ionic and electronic conductivity [39, 45, 56–60]. There have been many attempts to interpret the unique transport properties

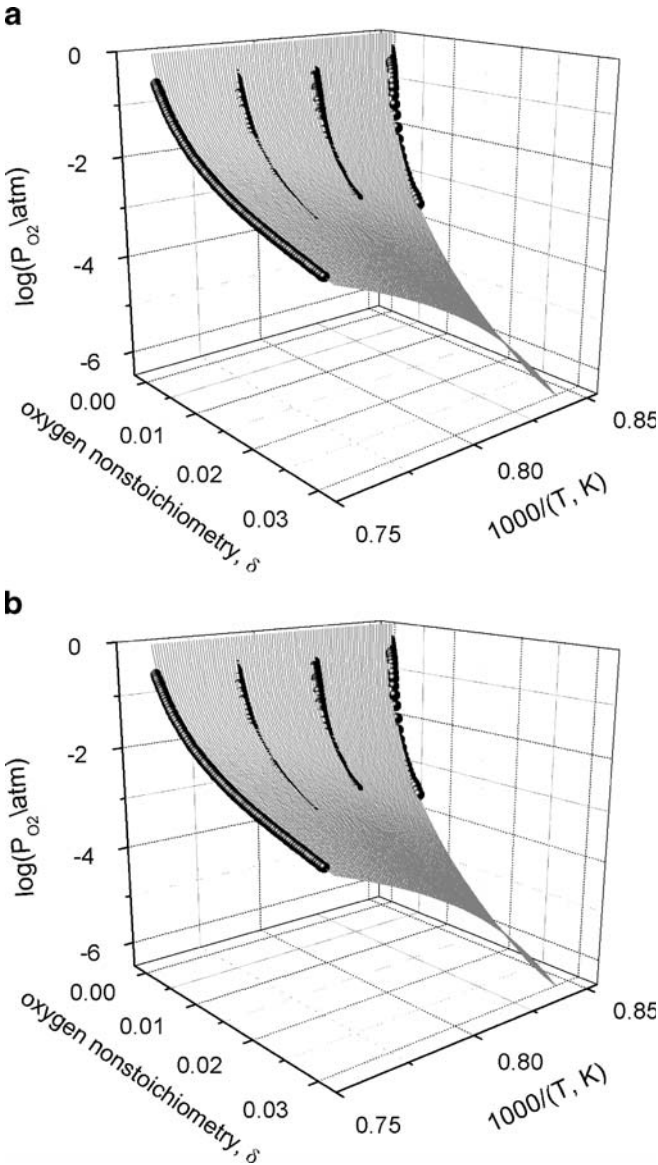


Fig. 16 **a** Oxygen nonstoichiometry of $\text{LaCoO}_{3-\delta}$ as a function of p_{O_2} and temperature. The fitted surface is plotted on the basis of defect model 1. **b** Oxygen nonstoichiometry of $\text{LaCoO}_{3-\delta}$ measured as a function of p_{O_2} and temperature. The fitted surface is plotted on the basis of defect model 2

of $\text{LaCo}_{1-y}\text{B}_y\text{O}_{3-\delta}$ [61–64] and $\text{La}_{1-x}\text{Sr}_x\text{Co}_{1-y}\text{B}_y\text{O}_{3-\delta}$ [50, 65] ($\text{B}=\text{Mn, Fe, Ni, and Cu}$), considering various conduction mechanisms and a variety of defect species and cobalt spin states. Raccah and Goodenough [56] first proposed a first-order localized-to-itinerant electron transition at 1,210 K based upon electrical measurements and differential thermal analysis results. Thornton et al. [66] suggested a gradual transition involving the thermal promotion of electrons from π^* band associated with the localized t_{2g} orbitals to the delocalized σ^* band associated with the e_g orbitals. Later, Goodenough et al. [67] proposed an evolutional, localized-to-itinerant electron transition

based on the presence of Co in different spin states, instead of a phase transition, to explain the magnetic and transport properties of lanthanum cobaltite-based oxides. This model did not account, however, the possibility of Co disproportionation. Contrarily, Sehlin et al. [58] explained the Seebeck coefficient and effective paramagnetic moments for $\text{LaCoO}_{3-\delta}$ on the basis of a semiempirical model involving the mechanism of charge disproportionation in the Co sublattice. Later, Kozhevnikov et al. [50], for $\text{La}_{0.7}\text{Sr}_{0.3}\text{Co}_{1-y}\text{Mn}_y\text{O}_{3-\delta}$, and Petrov et al. [63], for $\text{LaCo}_{0.7}\text{Cu}_{0.3}\text{O}_{3-\delta}$, applied the model mentioned above to interpret the electronic conductivity and Seebeck coefficient of these compounds. Thus, despite the intense activity and continuous interest over the past decades, the electronic structure and the conductivity mechanism in undoped and doped lanthanum cobaltites remain controversial topics of discussions. So far, researchers [56, 66, 67] have primarily interpreted the magnetic and transport properties of these cobaltites in terms of a transition from localized-to-itinerant electron state, focusing upon the presence of Co atoms in different spin states within the framework of band theory. This physical approach has a lot of problems regarding the definition of energy levels of 3d-transition atoms and oxygen, which in turn depend on crystal field, a degree of localization of conductive electronic species. However, there is an alternative approach within the framework of which the basic statements of a physical approach is supplemented by a thermodynamic description of equilibrium atomic and electronic defects [45, 57, 59, 63].

The electrical conductivities (σ) and Seebeck coefficients (Q) of $\text{LaCoO}_{3-\delta}$ (Petrov et al. submitted for publication), $\text{La}_{0.7}\text{Sr}_{0.3}\text{CoO}_{3-\delta}$ [50], $\text{La}_{0.4}\text{Sr}_{0.6}\text{CoO}_{3-\delta}$ [60], $\text{LaCo}_{0.7}\text{Cu}_{0.3}\text{O}_{3-\delta}$ [63], and $\text{La}_{0.7}\text{Sr}_{0.3}\text{Co}_{0.75}\text{Mn}_{0.25}\text{O}_{3-\delta}$ [50] are plotted vs oxygen partial pressure in Figs. 21a, 22a, 23a, 24a, and 25a, respectively. For the sake of comparison, the conductivity and Seebeck coefficients of all compounds are shown in Fig. 26 at 900 °C. It is noteworthy that the formation of oxygen vacancies in undoped $\text{LaCoO}_{3-\delta}$ does not lead to a significant change of its electrical conductivity and Seebeck coefficient, unlike doped lanthanum cobaltites. The substitutions of alkali-earth metals, for instance, Sr for La on A-site, and of 3d-transition metals, for instance, Mn or Cu for Co on B-site, result in substantial influence of the oxygen nonstoichiometry on electrical properties. In particular, a partial substitution of Sr for La on dodecahedral sites leads to an abrupt increase of electrical conductivity of lanthanum cobaltite, which reaches the maximum for $\text{La}_{0.7}\text{Sr}_{0.3}\text{CoO}_{3-\delta}$, and its Seebeck coefficient decrease, because Sr_{La}^+ is a typical electron acceptor. Partial substitution of Cu as an electron acceptor (Cu_{Co}^+) or Mn as an electron donor ($\text{Mn}_{\text{Co}}^{\bullet}$) for Co on octahedral sites results in a decrease of the overall conductivity. The positive values of the Seebeck coefficient seem to indicate that electronic holes are dominant charge carriers.

Table 2 The fitting results according to the defect structure models proposed for the lanthanum cobaltites

Compound	Reference	Temperature range (K)	Model	Reaction, Eq. (i)	$\Delta H_i^0(\pm\Delta)$, kJ/mol	$\ln(K^0)_i(\pm\Delta)$	R^2
LaCo _{3-δ}	Petrov et al., Submitted for publication	1,173–1,323	1	(9) (13)	468(±38) 638(±35)	39.7(±3.5) 47.3(±3.8)	0.979
			2	(11) (17)	691(±46) 518(±48)	52.8(±4.6) 45.0(±4.9)	0.979
		1,023–1,198	1	(9) (13)	195(±34) 117(±3)	79.3(±2.7) 119.2(±28.5)	0.973
			2	(11) (17)	140(±14) 397(±28)	231.4(±11.9) 78.2(±23.6)	0.987
La _{0.4} Sr _{0.6} CoO _{3-δ}	[60]	1,073–1,173	1	(9) (13)	43(±5) 127(±5)	−7.6(±5.1) 112.6(±4.5)	0.998
			2	(11) (17)	39(±4) 210(±5)	−7.5(±3.4) 98.2(±4.6)	0.994
		973–1,273	1A	(9) (13) (31)	197.3(−) −67.7(−) 98.5(−)	80.8(−) 5.5(−) 39.2(−)	0.989
			2A	(11) (29) (31)	176(−) 100(−) 102(−)	68.3(−) 33.4(−) 41.8(−)	0.990
La _{0.7} Sr _{0.3} Co _{0.75} Mn _{0.25} O _{3-δ}	[50]	1,073–1,173	1B	(9) (13) (41)	24.7(−) 153.0(−) 104.7(−)	−31.0(−) 127.2(−) 102.1(−)	0.996
			2B	(11) (43) (45)	99.3(−) 41.1(−) 181.6(−)	40.3(−) 37.4(−) 48.3	0.998

In the present work, the joint analyses of electrical conductivities and Seebeck coefficients of LaCo_{3- δ} , La_{0.7}Sr_{0.3}CoO_{3- δ} , La_{0.4}Sr_{0.6}CoO_{3- δ} , LaCo_{0.7}Cu_{0.3}O_{3- δ} , and La_{0.7}Sr_{0.3}Co_{0.75}Mn_{0.25}O_{3- δ} are carried out on the basis of their p_{O_2} –T– δ diagrams. The experimental isothermal dependencies $\log\sigma_T$ – $\log p_{O_2}$ and Q_T – $\log p_{O_2}$ were recalculated in $\log\sigma_T$ – δ and Q_T – δ using the isothermal sections ($\log p_{O_2}$)_T– δ , and are shown in Figs. 21b, 22b, 23b, 24b, and 25b.

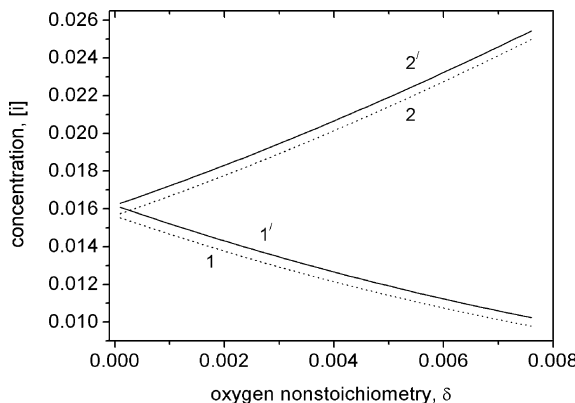


Fig. 17 Changes of concentration of different defect species in LaCo_{3- δ} at 900°C computed on the basis of the defect model 1 ($1p$ and $2n$) and model 2 ($1'[Co_{Co}^\bullet]$ and $2'[Co_{Co}^-]$)

According to previous studies, the conductivity of La_{1- x} A _{x} CoO_{3- δ} is realized by means of a charge transfer through the adjacent Co sites. The hopping (polaron) mechanism of this charge transfer is assumed in most cases [45, 56, 58–60, 63] (Petrov et al. submitted for publication). Nevertheless, there are only a few works dealing with a quantitative determination of the real nature of polarons (whether they are small- or large-radius polarons) and their

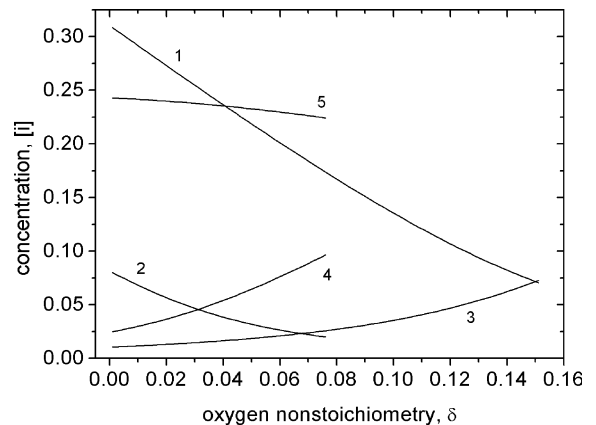


Fig. 18 Changes of concentration of different defect species at 900°C computed on the basis of the defect model 2B: in La_{0.7}Sr_{0.3}CoO_{3- δ} (1 [Co_{Co}^\bullet], 3 [Co_{Co}^-]); in La_{0.7}Sr_{0.3}Co_{0.75}Mn_{0.25}O_{3- δ} (2 [Co_{Co}^\bullet], 4 [Co_{Co}^-], and 5 [Mn_{Co}^\bullet]))

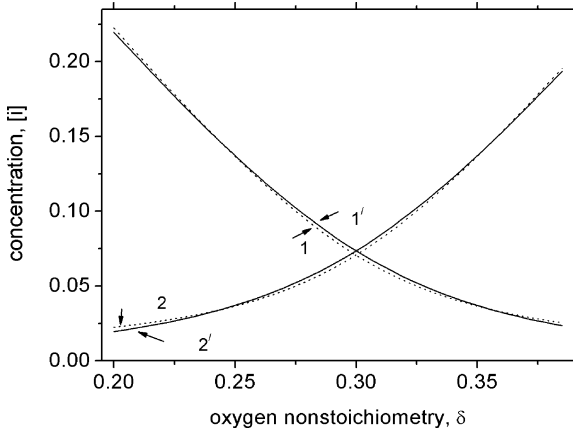


Fig. 19 Changes of concentration of different defect species in $\text{La}_{0.4}\text{Sr}_{0.6}\text{CoO}_{3-\delta}$ at $900\text{ }^\circ\text{C}$ computed on the basis of the defect model 1 ($1p$ and $2n$) and model 2 ($1'[\text{Co}_{\text{Co}}^{\bullet}]$ and $2'[\text{Co}_{\text{Co}}^{\prime\bullet}]$)

properties, such as concentration and mobility [50, 63] (Petrov et al. submitted for publication). In the case of the hopping mechanism of charge transfer, the temperature dependencies of conductivity and the Seebeck coefficient are described using well-known expressions [68]:

$$\sigma = \frac{A}{T} \exp \left(-\frac{W}{kT} \right) \quad (51)$$

and

$$Q_{\pm} = \pm \frac{k}{e} \left(\frac{E}{kT} + B \right), \quad (52)$$

where $W = (E + H_{\pm})$ and E are the activation energy of conductivity and the Seebeck coefficient, respectively. The value of E in both cases has the same origin and implies the

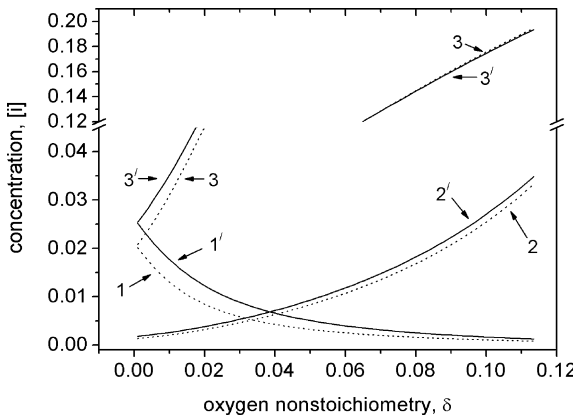


Fig. 20 Changes of concentration of different defect species in $\text{LaCo}_{0.7}\text{Cu}_{0.3}\text{O}_{3-\delta}$ at $900\text{ }^\circ\text{C}$ computed on the basis of the defect model 1A, model 1B ($1p$, $2n$, and $3[\text{Cu}_{\text{Co}}^{\prime\bullet}]$), and model 2A ($1'[\text{Co}_{\text{Co}}^{\bullet}]$, $2'[\text{Co}_{\text{Co}}^{\prime\bullet}]$, and $3'[\text{Cu}_{\text{Co}}^{\bullet}]$)

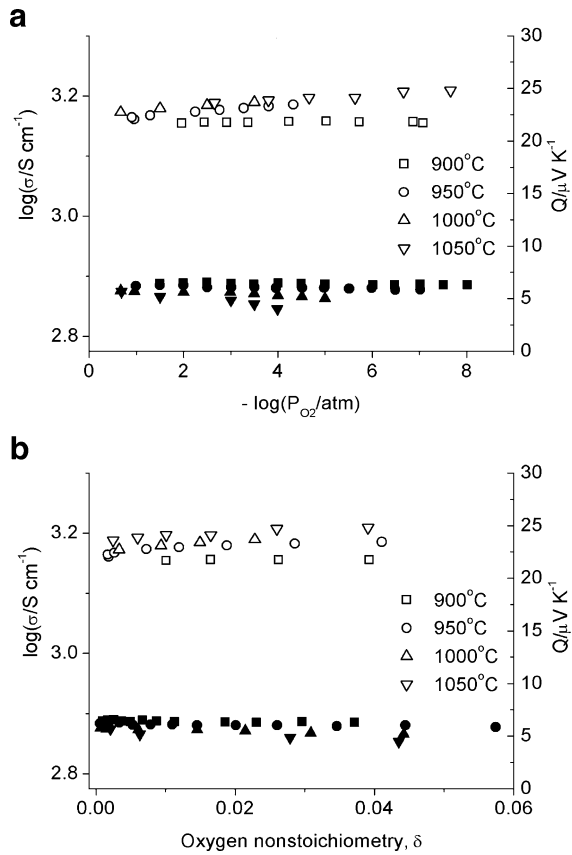


Fig. 21 The conductivity (filled symbols) and Seebeck coefficient (open symbols) of undoped lanthanum cobaltite $\text{LaCoO}_{3-\delta}$ (Petrov et al. submitted for publication) depending on: **a** oxygen partial pressure; **b** oxygen nonstoichiometry at different temperatures

ionization energy of a polaron. If the value of H_{\pm} is equal to 0, the charge transfer is believed to be unactivated and realized by large polarons. Otherwise, if $H_{\pm} \neq 0$, the charge transfer is regarded as thermal excited and realized by means of the hopping mechanism of small polarons.

The temperature dependencies of conductivity and the Seebeck coefficient are shown in Fig. 27 at fixed oxygen nonstoichiometry. The values of activation energy are given in Table 3. The highest activation energy ($0.54 \leq H_{\pm}$, $\text{eV} \leq 0.70$) is observed for cobaltite with high strontium content $\text{La}_{0.4}\text{Sr}_{0.6}\text{CoO}_{3-\delta}$. The last result is quite predictable because only this phase is semiconducting as mentioned above. The values of an activation energy of charge transfer in other phases are substantially lower and lie in the range $0.01 \leq H_{\pm}$, $\text{eV} \leq 0.17$. However, the positive sign of H_{\pm} indicates the hopping charge transfer by means of small polarons.

Thus, electrons and holes localized on the atoms of 3d-transition metals $\text{Co}_{\text{Co}}^{\bullet}$, $\text{Co}_{\text{Co}}^{\prime\bullet}$, $\text{Cu}_{\text{Co}}^{\prime\bullet}$, and $\text{Mn}_{\text{Co}}^{\bullet}$ can be treated as the dominant electronic defects, which are the primal charge carriers. The contribution of oxygen ionic conductivity seems to be negligible compared to that of the electronic conductivity because the oxygen transport number measured for $\text{LaCoO}_{3-\delta}$ at $1,000\text{ }^\circ\text{C}$ does not

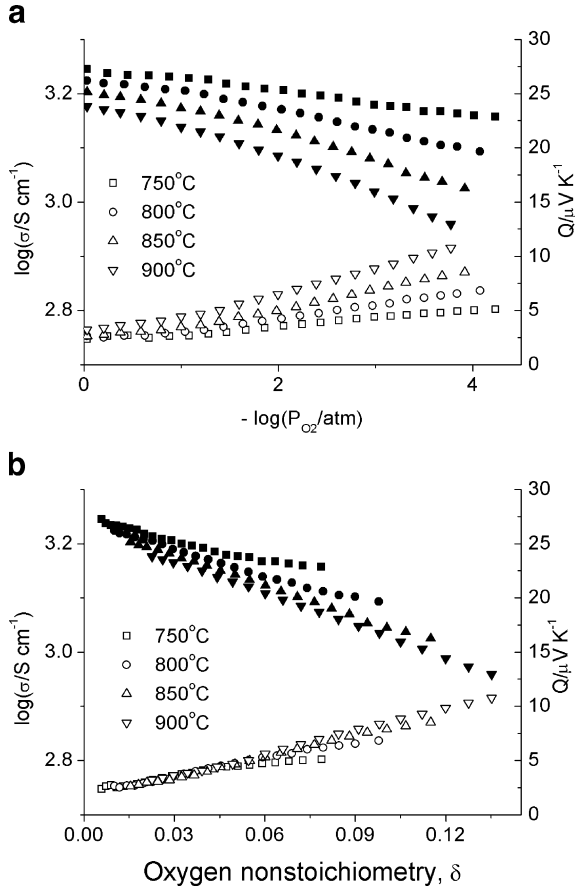


Fig. 22 The conductivity (filled symbols) and Seebeck coefficient (open symbols) of doped lanthanum cobaltite La_{0.7}Sr_{0.3}CoO_{3-δ} [50] depending on: **a** oxygen partial pressure; **b** oxygen nonstoichiometry at different temperatures

exceed the value of 10⁻⁵ [69]. The transport number of Sr_{La}⁺ in the lanthanum sublattice is less than that of oxygen by a few orders of magnitude. This allows us to assume that electrons (M_{Co}^- or neg) and holes (M_{Co}^+ or pos) localized on the 3d-transition metal cations contribute primarily to the total conductivity and thermopower. Then the electrical properties can be described as:

$$\sigma = \frac{a \cdot |e|}{V_a} \nu_e ([neg] + L \cdot [pos]) \quad (53)$$

$$Q = t_e Q_e + t_h Q_h = \frac{[neg] \cdot Q_e + L \cdot [pos] \cdot Q_h}{[neg] + L \cdot [pos]}, \quad (54)$$

where V_a is the volume of hexagonal unit cell (Table 4) [50, 63, 70] (Petrov et al. submitted for publication); a is the number of formula units per unit cell equal to 6; ν_e and ν_h are the mobilities of electron and hole, respectively; [neg] and [pos] are the concentrations of negative and positive polarons, respectively; Q_h and Q_e are the partial thermoelectric coefficients; t_e and t_h are the transport numbers of

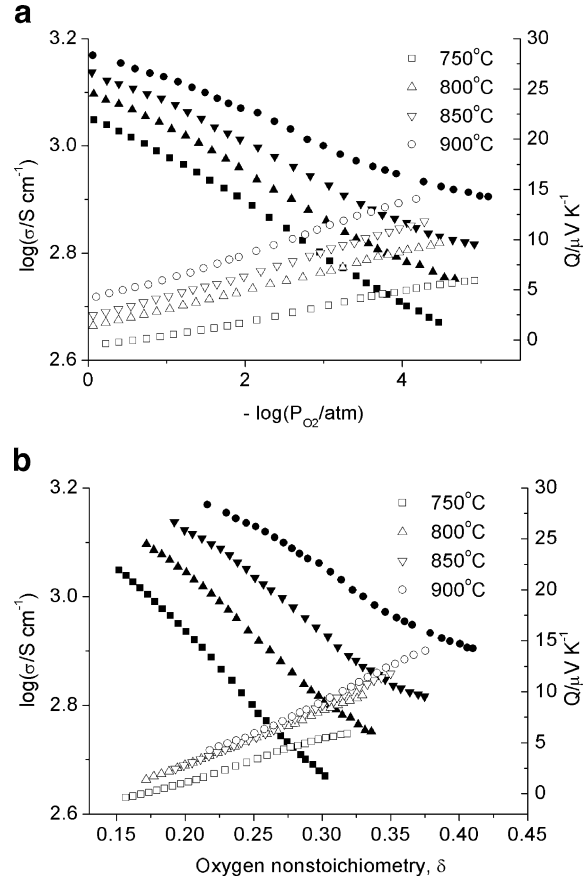


Fig. 23 The conductivity (filled symbols) and Seebeck coefficient (open symbols) of doped lanthanum cobaltite La_{0.4}Sr_{0.6}CoO_{3-δ} [60] depending on: **a** oxygen partial pressure; **b** oxygen nonstoichiometry at different temperatures

electron and hole, respectively; $L = \nu_h / \nu_e$ is the ratio of the mobilities.

In the model of localized carriers, Q_h and Q_e are given by the formulas [68]:

$$Q_h = \frac{k}{|e|} \left[\ln \left\{ \frac{1}{\beta_h} \frac{1 - [pos]}{[pos]} \right\} + \frac{S_{h*}}{k} \right] \quad (55)$$

$$Q_e = \frac{k}{|e|} \left[\ln \left\{ \beta_e \frac{1 - [neg]}{[neg]} \right\} + \frac{S_{e*}}{k} \right], \quad (56)$$

where $\beta_h = \frac{5}{6}$ and $\beta_e = \frac{4}{5}$ are the spin degenerate factors for cobalt ions Co^{IV} and Co^{II}, respectively [71]; k is the Boltzmann constant; $S_{h/e*} = \frac{H_{h/e*}}{T}$ is the vibrational entropy, and $H_{h/e*}$ is the enthalpy of transfer of hole/electron. The concentrations of negative- and positive-charged polarons for the cobaltites studied are defined as follows: for undoped LaCoO_{3-δ} and Sr-doped La_{1-x}Sr_xCoO_{3-δ} — [pos] = [Co_{Co}⁺] and [neg] = [Co_{Co}⁻], respectively; for copper-doped LaCo_{0.7}Cu_{0.3}O_{3-δ} — [pos] = [Co_{Co}⁺]

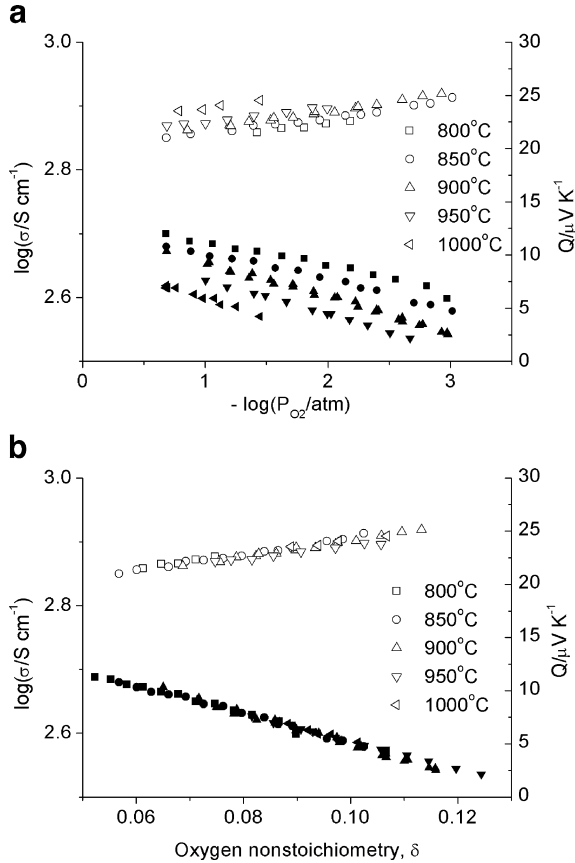


Fig. 24 The conductivity (filled symbols) and Seebeck coefficient (open symbols) of doped lanthanum cobaltite LaCo_{0.7}Cu_{0.3}O_{3-δ} [63] depending on: **a** oxygen partial pressure; **b** oxygen nonstoichiometry at different temperatures

and $[neg] = \left[Cu'_{Co} \right] + \left[Co'_{Co} \right]$, respectively; for La_{0.7}Sr_{0.3}Co_{0.75}Mn_{0.25}O_{3-δ} — $[pos] = \left[Co^{\bullet}_{Co} \right] + \left[Mn^{\bullet}_{Co} \right]$ and $[neg] = \left[Co'_{Co} \right]$, respectively.

The contribution of the vibrational entropy term $\frac{S_{h/e^*}}{e}$ to the overall Seebeck coefficient is usually negligible in comparison to that of the configurational entropy term $\frac{k}{|e|} \left[\ln \left\{ \frac{1-[pos]}{[pos]} \right\} \right]$, and the former is often neglected. Equations 53 and 54 contain the charge carrier concentrations determined in the previous section and mobilities of electrons ν_e and holes ν_h which are unknown a priori. Simultaneous analysis of Eqs. 53 and 54 and experimental values of σ and Q as a function of δ at given T allows us to determine the unknown parameters ν_e , or ν_h and L for each cobaltite composition studied by solving the following set of equations:

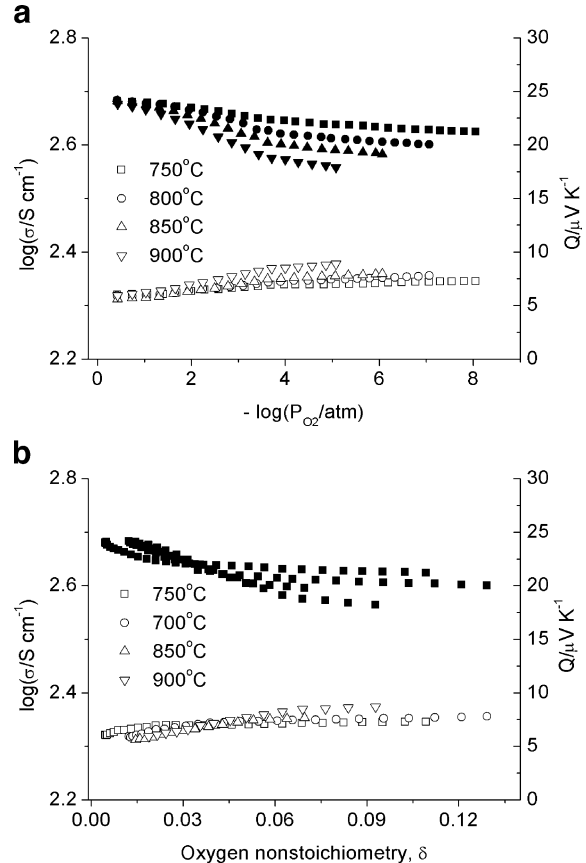


Fig. 25 The conductivity (filled symbols) and Seebeck coefficient (open symbols) of doped lanthanum cobaltite La_{0.7}Sr_{0.3}Co_{0.75}Mn_{0.25}O_{3-δ} [50] depending on: **a** oxygen partial pressure; **b** oxygen nonstoichiometry at different temperatures

$$\left. \begin{aligned} \sigma_T(\delta) &= \frac{a \cdot |e|}{V_a} \nu_e ([neg]_T + L \cdot [pos]_T) = F_1(\nu_e, L, \delta) \\ Q_T(\delta) &= \frac{[neg]_T \cdot Q_e + L \cdot [pos]_T \cdot Q_h}{[neg]_T + L \cdot [pos]_T} = F_2(L, \delta) \end{aligned} \right\} \quad (57)$$

The results are given in Table 5 and Figs. 28, 29, 30, and 31. Figure 28 shows the dependencies of concentration and mobility of different polarons on oxygen nonstoichiometry for undoped LaCoO_{3-δ} and Cu-doped LaCo_{0.7}Cu_{0.3}O_{3-δ} at 900 °C. The concentration of localized holes is equal to that of localized electrons (Fig. 17) and comes to a value of 0.016 in the stoichiometric LaCoO₃ at 900 °C, whereas the mobilities of holes and electrons is slightly different, 8.462 and 8.263 cm²V⁻¹s⁻¹, respectively. The mobility of a localized hole $[Co^{\bullet}_{Co}]_T$ (Fig. 28) increases with oxygen nonstoichiometry, whereas that of localized electrons $[Co'_{Co}]_T$ decreases.

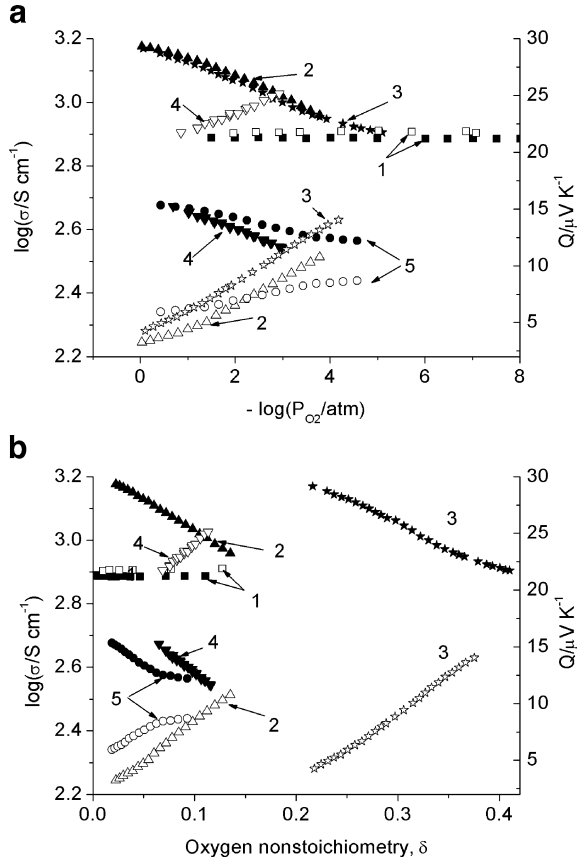


Fig. 26 The conductivity (filled symbols) and Seebeck coefficient (open symbols) of the lanthanum cobaltite: *1*LaCoO_{3-δ}, *2*La_{0.7}Sr_{0.3}CoO_{3-δ}, *3*La_{0.4}Sr_{0.6}CoO_{3-δ}, *4*LaCo_{0.7}Cu_{0.3}O_{3-δ}, and *5*La_{0.7}Sr_{0.3}Co_{0.75}Mn_{0.25}O_{3-δ} at 900°C depending on: **a** oxygen partial pressure; **b** oxygen nonstoichiometry

To explain the behavior mentioned above, one should account that the metallic conductivity is caused by a partial rearrangement of valent electrons of the cobalt ions Co³⁺ of the CoO₆ octahedra. These cobalt species switch their spin from high spin $t_{2g}^4 e_g^2$ to low spin $t_{2g}^6 e_g^0$. Such a rearrangement induces a disproportionation of the two nearest ions Co³⁺ of the octahedra CoO₆ according to reaction Eq. 11 and, therefore, facilitates electron hopping from Co³⁺ to an adjacent Co⁴⁺ neighbor through a *p* oxygen orbital [72]. Oxygen partial pressure decrease causes the growth in oxygen deficit in the oxide due to the oxygen vacancies ($V_O^{••}$) formation, that in the localized electrons concentration Co_{Co}^{\prime} , and, consequently, reduction of the localized holes ($[Co_{Co}^{\bullet}]_T$). The vacancies may act as traps for the mobile electrons. As a consequence, the mobility of the negatively charged polarons has to drop due to formation of the immobile clusters $(V_O^{••} - Co_{Co}^{\prime})^{\bullet}$ as the oxygen nonstoichiometry increases, although their concentration increases due to the reaction Eq. 14 at the same time. On the other hand, the Co³⁺ species of the CoO₅ pyramids (where one vertex of the octahedra CoO₆ is vacant) is in the $t_{2g}^5 e_g^1$ configuration, the intermediate spin

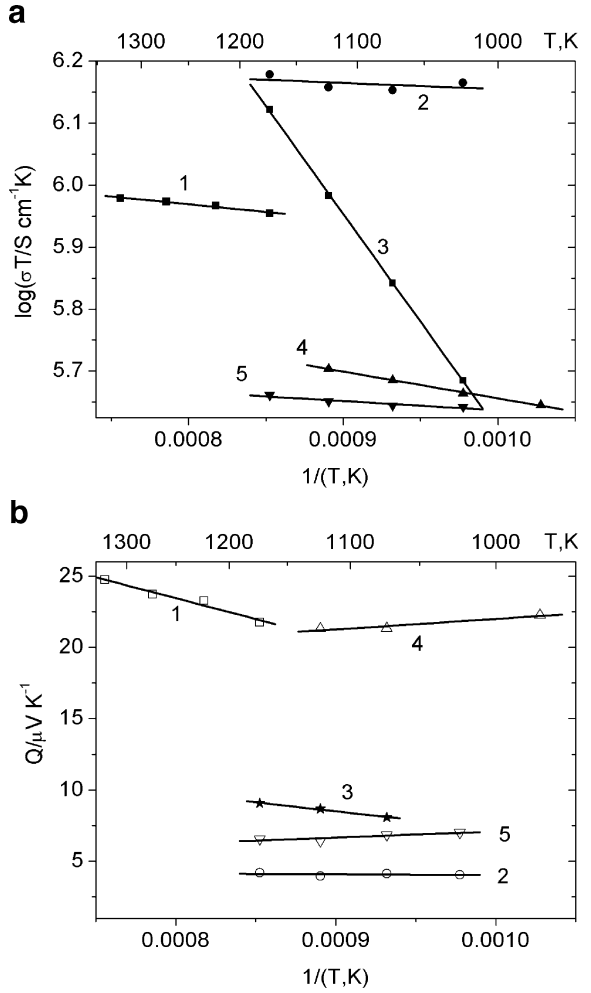


Fig. 27 The conductivity and Seebeck coefficient of the lanthanum cobaltite: *1*LaCoO_{3-δ} ($\delta=0.03$), *2*La_{0.7}Sr_{0.3}CoO_{3-δ} ($\delta=0.04$), *3*La_{0.4}Sr_{0.6}CoO_{3-δ} ($\delta=0.3$), *4*LaCo_{0.7}Cu_{0.3}O_{3-δ} ($\delta=0.06$), *5*La_{0.7}Sr_{0.3}Co_{0.75}Mn_{0.25}O_{3-δ} ($\delta=0.03$) as functions of reciprocal temperature

state. Hence, the disproportionation of the two nearest ions Co³⁺ of the pyramids CoO₅ according to reaction Eq. 11 becomes energy-hindered. This hampers electron hopping from Co³⁺ to an adjacent Co⁴⁺ neighbor through a *p* oxygen orbital.

The partial substitution of copper for cobalt with the formation of the electron acceptor Cu_{Co}⁺ facilitates the oxygen vacancy formation, but does not influence the aforementioned disproportionation in general. Figures 20 and 28 show that the trend in the electronic species concentration vs oxygen nonstoichiometry remains essentially unchanged when cobalt is substituted by copper, whereas the absolute values change. Nevertheless, the presence of copper atoms (Cu_{Co}⁺), which are more electronegative than those of cobalt and, therefore, can be regarded as the hole (Co_{Co}[•]) trappings, in the structure of LaCo_{0.7}Cu_{0.3}O_{3-δ} induces the reduction of the hole mobility, as compared with undoped LaCoO_{3-δ}. The excess of the mobility of positive-charged polarons

Table 3 The values of energetic parameters for charge transfer

Composition	δ	W, eV	E, eV	H_{\pm} , eV
LaCoO _{3-δ}	0.02	0.055(5)	-0.026(4)	0.081(5)
LaCoO _{3-δ}	0.03	0.049(5)	-0.029(4)	0.078(5)
LaCoO _{3-δ}	0.04	0.044(5)	-0.028(7)	0.072(5)
La _{0.7} Sr _{0.3} CoO _{3-δ}	0.02	0.035(1)	0.0001(3)	0.035(1)
La _{0.7} Sr _{0.3} CoO _{3-δ}	0.04	0.032(6)	-0.0001(3)	0.032(6)
La _{0.7} Sr _{0.3} CoO _{3-δ}	0.06	0.02(2)	0.0001(3)	0.01(2)
La _{0.4} Sr _{0.6} CoO _{3-δ}	0.2	0.52(5)	-0.021(2)	0.54(5)
La _{0.4} Sr _{0.6} CoO _{3-δ}	0.25	0.62(6)	-0.006(1)	0.62(6)
La _{0.4} Sr _{0.6} CoO _{3-δ}	0.3	0.69(7)	-0.012(2)	0.70(7)
LaCo _{0.7} Cu _{0.3} O _{3-δ}	0.06	0.085(3)	0.007(1)	0.079(3)
LaCo _{0.7} Cu _{0.3} O _{3-δ}	0.07	0.12(2)	0.006(1)	0.11(2)
LaCo _{0.7} Cu _{0.3} O _{3-δ}	0.08	0.15(1)	0.0056(6)	0.14(1)
LaCo _{0.7} Cu _{0.3} O _{3-δ}	0.09	0.14(2)	0.0068(8)	0.13(2)
La _{0.7} Sr _{0.3} Co _{0.75} Mn _{0.25} O _{3-δ}	0.02	0.175(3)	0.007(2)	0.168(3)
La _{0.7} Sr _{0.3} Co _{0.75} Mn _{0.25} O _{3-δ}	0.03	0.133(7)	0.004(2)	0.129(7)
La _{0.7} Sr _{0.3} Co _{0.75} Mn _{0.25} O _{3-δ}	0.04	0.09(1)	0.001(2)	0.089(1)
La _{0.7} Sr _{0.3} Co _{0.75} Mn _{0.25} O _{3-δ}	0.05	0.06(1)	-0.004(1)	0.064(1)
La _{0.7} Sr _{0.3} Co _{0.75} Mn _{0.25} O _{3-δ}	0.06	0.04(1)	-0.007(1)	0.047(1)

(Co_{Co}^{\bullet}) over that of negative-charged polarons (Co_{Co}^{\bullet} Or Cu_{Co}^{\prime} + Co_{Co}^{\prime}) seems to be a noteworthy feature for both lanthanum cobaltites. The value of $L=(\nu_h/\nu_e)$ exceeds unity and changes within the ranges $1 \leq L \leq 22$ and $14 \leq L \leq 32$ for LaCoO_{3- δ} and La_{0.7}Sr_{0.3}CoO_{3- δ} , respectively, as the oxygen nonstoichiometry increases (see Fig. 31).

Isothermal dependencies of the mobility (Fig. 30) and concentration of the charge carriers (Figs. 18 and 19) vs oxygen nonstoichiometry for Sr-doped cobaltites La_{1-x}Sr_xCoO_{3- δ} ($x=0.3, 0.6$) differ from those of undoped LaCoO_{3- δ} (see Figs. 17 and 29). It is seen that substitution of Sr for La in LaCoO_{3- δ} leads to a noticeable increase of hole concentration and a change of the sign of the most mobile polaron. Note that the concentration of localized holes Co_{Co}^{\bullet} exceeds that of localized electrons Co_{Co}^{\prime} by more than one order of magnitude in the stoichiometric composition of La_{0.7}Sr_{0.3}CoO₃ with respect to oxygen ($\delta=0$) at 900 °C, unlike undoped LaCoO₃, and comes to the value of 0.310. At the same time, the values of mobility of localized holes and electrons come to 1.526 and 9.963 cm²*V⁻¹*s⁻¹, respectively. The value of $L=(\nu_h/\nu_e)$ is less than

unity and comes to 0.153 at 900 °C for the stoichiometric La_{0.7}Sr_{0.3}CoO₃ with respect to oxygen. This aforementioned change of the sign is most likely caused by a braking of holes at the doped sites Sr_{La}^{\prime} and formation of the neutral clusters $(Sr_{La}^{\prime} - Co_{Co}^{\bullet})^x$. The role of oxygen vacancies is to increase the trappings of electrons, and the electrons' mobility, therefore, drops as the oxygen nonstoichiometry increases up to a value of 2.163 cm²*V⁻¹*s⁻¹ at $\delta=0.15$ and 900 °C. Simultaneously, the mobility of holes Co_{Co}^{\bullet} increases somewhat, reaching a value of 2.043 cm²*V⁻¹*s⁻¹ at $\delta=0.15$ and 900 °C. The concentration of the localized holes becomes equal to that of the localized electrons and comes to a value of 0.072 when oxygen nonstoichiometry of La_{0.7}Sr_{0.3}CoO_{3- δ} reaches a value of 0.15 at 900 °C (see Fig. 30).

An analogous situation is observed for La_{0.4}Sr_{0.6}CoO_{3- δ} (see Fig. 30). In this case, a change of the “leader” of charge transfer occurs about a point with $\delta=0.3$ at 900 °C within the range of oxygen nonstoichiometry investigated. In this point, the concentration of localized holes becomes equal to that of localized electrons and comes to a value of 0.0756. At the same time, the mobility of the former is equal to the value of 2.539 cm²*V⁻¹*s⁻¹, whereas that of the latter comes to 2.747 cm²*V⁻¹*s⁻¹.

Partial substitution of Mn for Co does not significantly change the nature of charge transfer in La_{0.7}Sr_{0.3}Co_{0.75}Mn_{0.25}O_{3- δ} in comparison with La_{0.7}Sr_{0.3}CoO_{3- δ} , despite the fact that manganese is obviously a donor of electrons (see Fig. 30). Localized electrons Co_{Co}^{\prime} remain the most mobile species in La_{0.7}Sr_{0.3}Co_{0.75}Mn_{0.25}O_{3- δ} , but their mobility is somewhat less than that in La_{0.7}Sr_{0.3}CoO_{3- δ} . The overall mobility of Co_{Co}^{\bullet} and Mn_{Co}^{\bullet} as positive charged polarons in La_{0.7}Sr_{0.3}Co_{0.75}Mn_{0.25}O_{3- δ} is also less than that of Co_{Co}^{\bullet} in La_{0.7}Sr_{0.3}CoO_{3- δ} .

Table 4 Unit cell volumes of the lanthanum cobaltites

Composition	V, Å ³	Reference
LaCoO ₃	336.03 (5)	Petrov et al. (submitted for publication)
La _{0.7} Sr _{0.3} CoO ₃	340.00 (4)	[70]
LaCo _{0.7} Cu _{0.3} O ₃	340.57(3)	[63]
La _{0.7} Sr _{0.3} Co _{0.75} Mn _{0.25} O _{3-δ}	338.95 (3)	[70]
La _{0.4} Sr _{0.6} CoO _{3-δ}	341.0 (5)	[49]

Table 5 Calculated values of polaron mobility ($\text{cm}^2 \cdot \text{V}^{-1} \cdot \text{S}^{-1}$) for different temperature at fixed values of oxygen nonstoichiometry

	T, K	$(\nu_e)_{\delta=0.03}$	$(\nu_h)_{\delta=0.03}$	$(\nu_e)_{\delta=0.04}$	$(\nu_h)_{\delta=0.04}$
LaCoO _{3-δ}	1,173	2.782	22.990	2.249	27.670
LaCoO _{3-δ}	1,223	1.840	4.398	1.617	4.915
LaCoO _{3-δ}	1,273	0.990	1.384	0.934	1.428
LaCoO _{3-δ}	1,323	0.569	0.656	0.558	0.650
	T	$(\nu_e)_{\delta=0.07}$	$(\nu_h)_{\delta=0.07}$	$(\nu_e)_{\delta=0.08}$	$(\nu_h)_{\delta=0.08}$
LaCo _{0.7} Cu _{0.3} O _{3-δ}	1,073	0.894	32.374	0.763	36.139
LaCo _{0.7} Cu _{0.3} O _{3-δ}	1,123	0.868	19.141	0.745	21.080
LaCo _{0.7} Cu _{0.3} O _{3-δ}	1,173	0.851	12.270	0.726	13.224
LaCo _{0.7} Cu _{0.3} O _{3-δ}	1,223	—	—	0.704	8.630
LaCo _{0.7} Cu _{0.3} O _{3-δ}	1,273	—	—	0.683	6.107
	T	$(\nu_e)_{\delta=0.07}$	$(\nu_h)_{\delta=0.07}$	$(\nu_e)_{\delta=0.08}$	$(\nu_h)_{\delta=0.08}$
La _{0.7} Sr _{0.3} CoO _{3-δ} ,	1,023	33.102	2.264	29.377	2.413
La _{0.7} Sr _{0.3} CoO _{3-δ} ,	1,073	16.074	1.931	13.947	1.981
La _{0.7} Sr _{0.3} CoO _{3-δ} ,	1,123	8.802	1.736	7.616	1.743
La _{0.7} Sr _{0.3} CoO _{3-δ} ,	1,173	5.662	1.635	5.089	1.664
	T	$(\nu_e)_{\delta=0.2}$	$(\nu_h)_{\delta=0.2}$	$(\nu_e)_{\delta=0.4}$	$(\nu_h)_{\delta=0.4}$
La _{0.4} Sr _{0.6} CoO _{3-δ} ,	1,023	8.797	1.104	0.600	3.475
La _{0.4} Sr _{0.6} CoO _{3-δ} ,	1,073	8.418	1.379	0.739	3.660
La _{0.4} Sr _{0.6} CoO _{3-δ} ,	1,123	7.879	1.598	0.810	3.259
La _{0.4} Sr _{0.6} CoO _{3-δ} ,	1,173	7.071	1.742	0.996	3.348
	T	$(\nu_e)_{\delta=0.06}$	$(\nu_h)_{\delta=0.06}$	$(\nu_e)_{\delta=0.08}$	$(\nu_h)_{\delta=0.08}$
La _{0.7} Sr _{0.3} Co _{0.75} Mn _{0.25} O _{3-δ}	1,123	0.676	0.383	0.599	0.372
	1,173	0.595	0.654	0.532	0.709

Figure 31 shows the isothermal ratio of the mobilities of positive- and negative-charged polarons L in the oxides studied depending on their oxygen nonstoichiometry at 900 °C. It is seen that this value exceeds unity for undoped LaCoO_{3- δ} and doped with copper LaCo_{0.7}Cu_{0.3}O_{3- δ} , whereas this value is less than unity for doped with strontium cobaltite La_{0.7}Sr_{0.3}CoO_{3- δ} . Eventually, the value of L changes from 0.199 at $\delta=0.0175$ up to 3.92 at $\delta=0.42$ for La_{0.4}Sr_{0.6}CoO_{3- δ} , indicating, obviously, the

change of the nature of the most mobile charge carrier with that of oxygen nonstoichiometry.

Conclusions

The phase equilibria in the La–Me–Co–T–O (Me=Ca, Sr, Ba; T=Mn, Fe, Ni, Cu) systems were analyzed. The thermodynamic stability and the homogeneity ranges of

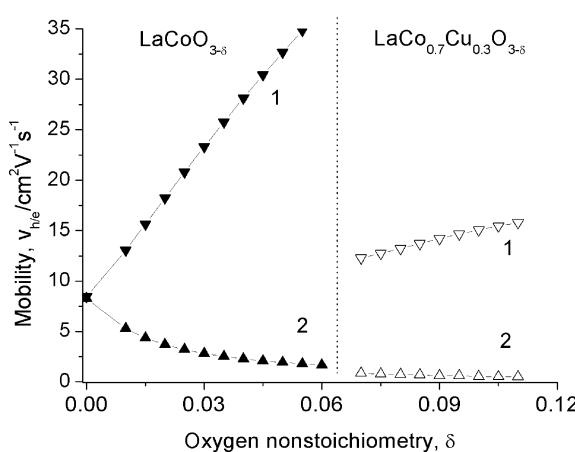


Fig. 28 Isothermal (900 °C) dependencies of the mobility for undoped LaCoO_{3- δ} (filled points) and for Cu-doped LaCo_{0.7}Cu_{0.3}O_{3- δ} vs oxygen nonstoichiometry (δ). Mobilities of positive (ν_h) (curve 1) and negative (ν_e) (curve 2) polarons

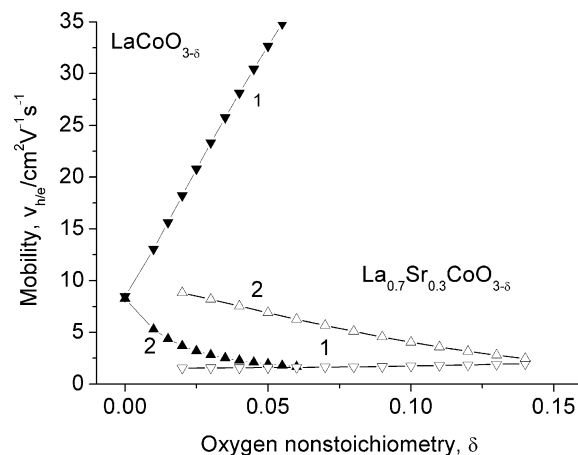


Fig. 29 Isothermal (900 °C) dependencies of the mobility for undoped LaCoO_{3- δ} (filled points) and for Sr-doped La_{0.7}Sr_{0.3}CoO_{3- δ} (open triangles) vs oxygen nonstoichiometry (δ). Mobilities of positive (ν_h) (curve 1) and negative (ν_e) (curve 2) polarons

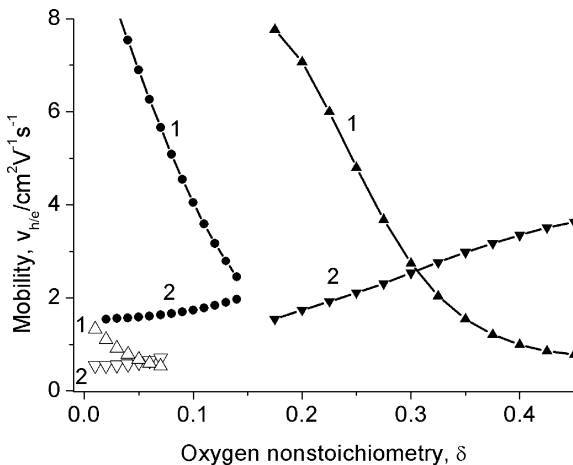


Fig. 30 Isothermal (900 °C) dependencies of the mobility for $\text{La}_{0.7}\text{Sr}_{0.3}\text{CoO}_{3-\delta}$ (filled points), $\text{La}_{0.4}\text{Sr}_{0.6}\text{CoO}_{3-\delta}$ (filled triangles), and Sr- and Mn-doped $\text{La}_{0.7}\text{Sr}_{0.3}\text{Co}_{0.75}\text{Mn}_{0.25}\text{O}_{3-\delta}$ vs oxygen nonstoichiometry (δ). Mobilities of positive (ν_h) (curve 2) and negative (ν_e) (curve 1) polarons

solid solutions are both significantly influenced by the nature of 3d-transition metal, particularly by their favorable oxidation states. The modeling of the defect structure of the oxygen-deficient lanthanum cobaltites, namely, undoped $\text{LaCoO}_{3-\delta}$, acceptor-doped in the A-sublattice [$\text{La}_{1-x}\text{Sr}_x\text{CoO}_{3-\delta}$ ($x=0.3, 0.6$)] and Cu-doped on the B-sites ($\text{LaCo}_{0.7}\text{Cu}_{0.3}\text{O}_{3-\delta}$), and doped simultaneously with Sr as the acceptor on A-site and Mn as a donor on B-site ($\text{La}_{0.7}\text{Sr}_{0.3}\text{Co}_{0.75}\text{Mn}_{0.25}\text{O}_{3-\delta}$), was carried out, considering both itinerant and localized electronic defects. The thermal-excited charge disproportionation of cobalt and intrinsic electronic disordering process (creation/annihilation of quasi-free holes and electrons) were taken into account as well. The analytical solution of a set of independent equations yielded a general expression, which can be used for fitting the experimental $p_{O_2}-T-\delta$ diagrams. The models of the defect structure based on the itinerant and localized nature of electronic defects all fitted the experimental data on oxygen nonstoichiometry about equally well. The charge transfer mechanism was identified

in the framework of localized charge carrier approach, using the results of defect structure and the data on electronic conductivity and the Seebeck coefficient. Analysis of the isoconcentration dependencies of conductivity ($\log \sigma_\delta = f(1/T)$) and those of the Seebeck coefficient $Q_\delta = f(1/T)$ revealed that charge transfer has the activation character for all oxides studied. These results evidences small polarons Co_{Co}^\bullet , $\text{Co}_{Co}^/$, $\text{Cu}_{Co}^/$, and Mn_{Co}^\bullet as the charge carriers in these oxides. Doping of the matrix cobaltite with acceptor dopants on A- and B-sites was shown to lead to different results depending on the nature and site of the dopant. For instance, doping with copper on B-site does not change the character of dependencies of the mobilities concentration of small polarons on the oxygen nonstoichiometry. In contrast, partial substitution of Sr for La in lanthanum cobaltite leads to a change of the dominant carriers with respect to their concentration and mobility, as compared to undoped $\text{LaCoO}_{3-\delta}$. Thus, negative-charged polaron $\text{Co}_{Co}^/$ has a higher mobility than that of positive-charged polaron Co_{Co}^\bullet .

Acknowledgements This work was supported by the Russian Foundation for Basic Research [grant numbers 04-03-32118, 05-03-32477, 04-03-96136 (Ural) and 04-03-32142], the Civilian Research & Development Foundation, and the Ministry of Education and Science of Russian Federation (project EK-005-XI).

References

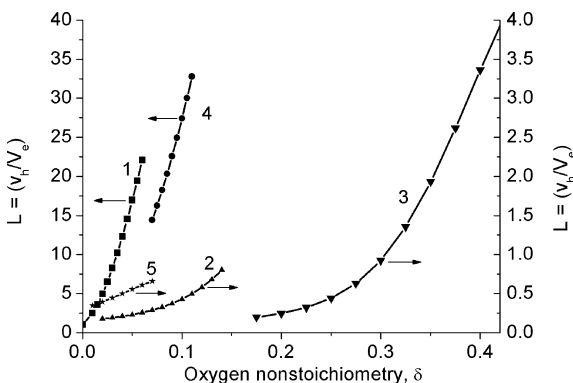


Fig. 31 The ratio of mobility for the positive and negative polarons at 900 °C for: 1 $\text{LaCoO}_{3-\delta}$, 2 $\text{La}_{0.7}\text{Sr}_{0.3}\text{CoO}_{3-\delta}$, 3 $\text{La}_{0.4}\text{Sr}_{0.6}\text{CoO}_{3-\delta}$, 4 $\text{La}_{0.7}\text{Cu}_{0.3}\text{O}_{3-\delta}$, 5 $\text{La}_{0.7}\text{Sr}_{0.3}\text{Co}_{0.75}\text{Mn}_{0.25}\text{O}_{3-\delta}$

1. Janecek JJ, Wirtz GP (1978) J Am Chem Soc 61:242
2. Seppanen M, Kyto M, Taskinen P (1979) Scand J Metal 8:199
3. Petrov AN, Cherepanov VA, Novitsky EM, Zhukovsky VM (1984) Russ J Phys Chem 58:1618
4. Petrov AN, Cherepanov VA, Zuyev AYu, Zhukovsky VM (1988) J Solid State Chem 75:1
5. Kitayama K (1997) J Solid State Chem 131:18
6. Borlera ML, Abbattista F (1983) J Less-Common Met 92:55
7. Nakamura T, Petzow G, Gauckel LJ (1979) Mater Res Bull 14:649
8. Kamigashira N, Miyazaki Y, Hiyoshi Y (1984) Mater Lett 2:194
9. Kamigashira N, Miyazaki Y (1984) Mater Chem Phys 11:187
10. Tretyakov YuD, Kaul AR, Portnoy VK (1977) High Temp Sci 9:61
11. Cherepanov VA, Barkhatova LYu, Petrov AN (1994) J Phys Chem Solids 55:229
12. Cherepanov VA, Barkhatova LYu, Petrov AN, Voronin VI (1995) In: Dokuya M, Yamamoto O, Tagawa H, Singhal SC (eds) Solid oxide fuel cells IV, PV 95-1. The Electrochemical Society, Pennington, pp 434
13. Cherepanov VA, Gavrilova LYa, Barkhatova LYu, Voronin VI, Trifonova MV, Bukhner OA (1998) Ionics 4:309
14. Cherepanov VA, Gavrilova LYa, Filonova EA, Trifonova MV, Voronin VI (1999) Mater Res Bull 34:983
15. Gavrilova LYa, Cherepanov VA, Surova TV, Baimistruk VA, Voronin VI (2002) Russ J Phys Chem 76:150
16. Gavrilova LYa, Cherepanov VA (1999) In: Singhal SC, Dokuya M (eds) Solid oxide fuel cells VI, PV 99-17. The Electrochemical Society Proceedings Series. The Electrochemical Society, Pennington, pp 404
17. Cherepanov VA, Gavrilova LYa, Petrov AN, Zuev AYu (2002) Z Anorg Allg Chem 628:2140
18. Zinkevich M, Aldinger F (2004) J Alloys Compd 375:147

19. Zhang Z, Greenblatt M, Goodenough JB (1994) *J Solid State Chem* 108:402
20. Bannikov DO, Cherepanov VA (2002) *Z Anorg Allg Chem* 628:2180
21. Cherepanov VA, Petrov AN, Grimova LYu, Novitsky EM (1983) *Russ J Phys Chem* 57:859 (in Russian)
22. Voronin VI, Berger IF, Cherepanov VA, Gavrilova LYa, Petrov AN, Ancharov AI, Tolochko BP, Nikitenko SG (2001) *Nucl Instrum Methods Phys Res A* 470:202
23. Petrov AN, Zuev AYu, Cherepanov VA, Kropanev AYu (1987) *Izv Akad SSSR Neorgan Mater* 23:949 (in Russian)
24. Skakle JMS, West AR (1994) *J Am Ceram Soc* 77:2199
25. Demazeau G, Marbeuf A, Pouchard M, Hagenmuller P (1971) *J Solid State Chem* 3:582
26. Gavrilova LYa, Proskurnina NV, Cherepanov VA, Voronin VI (2001) In: Yokokawa H, Singhal SC (eds) *Solid oxide fuel cells VII*, PV 2001-16. The Electrochemical Society Proceedings Series. The Electrochemical Society, Pennington, pp 458–465
27. Gopalakrishnan J, Colsmann G, Reuter B (1976) *Z Anorg Allg Chem* 424:155
28. Sawada H, Hamada N, Terakura K (1995) *J Phys Chem Solids* 56:1755
29. Tikhonova IL, Bakhtin AV, Zuev AYu, Petrov AN (1999) *Russ J Phys Chem* 73:365
30. Filonova EA, Cherepanov VA, Voronin VI (1998) *Russ J Phys Chem* 72:1706
31. Proskurnina NV, Shabunina OS, Cherepanov VA (2002) *Z Anorg Allg Chem* 628:2164
32. Proskurnina NV, Cherepanov VA, Golynets OS, Voronin VI (2004) *Inorg Mater* 40:955
33. Cherepanov VA, Filonova EA, Voronin VI, Berger IF, Barkhatova LYu (1999) *Mater Res Bull* 34:1481
34. Cherepanov VA, Filonova EA, Voronin VI, Berger IF (2000) *J Solid State Chem* 153:205
35. Cherepanov VA, Barkhatova LYu, Voronin VI (1997) *J Solid State Chem* 134:38
36. Aksanova TV, Gavrilova LYa, Cherepanov VA (2004) *Inorg Mater* 40:1336
37. Gavrilova LYa, Teslenko YaV, Bannikch LA, Aksanova TV, Cherepanov VA (2002) *J Alloys Compd* 344:28
38. Bobina MA, Yakovleva NA, Gavrilova LYa, Cherepanov VA (2004) *Russ J Phys Chem* 78:1340
39. Jonker GH (1969) *Philips Res Rep* 24:1
40. Zuev AYu, Petrov AN, Pankov DV (1999) In: Singhal SC, Dokia M (eds) *Solid oxide fuel cells VI*, PV 99-17. The Electrochemical Society Proceedings Series. The Electrochemical Society, Pennington, pp 424–431
41. Yasumoto K, Inagaki Y, Shiono M, Dokiya M (2002) *Solid State Ion* 148:545
42. Matsura T, Tabuchi J, Mizusaki J, Yamauchi S, Fueki K (1988) *J Phys Chem Solids* 49:1403
43. Mizusaki J, Mima Y, Yamauchi S, Fueki K, Tagawa H (1989) *J Solid State Chem* 80:102
44. Petrov AN, Cherepanov VA, Kononchuk OF, Gavrilova LYa (1990) *J Solid State Chem* 87:69
45. Petrov AN, Kononchuk OF, Andreev AV, Cherepanov VA, Kofstad P (1995) *Solid State Ion* 80:189
46. Lankhorst MHR, Bouwmeester HJM, Verweij H (1996) *Phys Rev Lett* 77:2989
47. Lankhorst MHR, Bouwmeester HJM, Verweij H (1997) *J Solid State Chem* 133:555
48. Lankhorst MHR, Bouwmeester HJM, Verweij H (1997) *Solid State Ion* 96:21
49. Patrakeev MV, Leonidov IA, Mitberg EB, Lakhtin AA, Vasiliev VG, Kozhevnikov VL, Poeppelmeier KR (1999) *Ionics* 5:444
50. Kozhevnikov VL, Leonidov IA, Mitberg EB, Patrakeev MV, Petrov AN, Poeppelmeier KR (2003) *J Solid State Chem* 172:296
51. Petrov AN, Zuev AYu, Pankov DV, Bujanova ES (2004) *Russ J Phys Chem* 78:220
52. Petrov AN, Zuev AYu, Pankov DV (2004) *Russ J Phys Chem* 78:1616
53. Seppanen M, Kyto M, Taskinen P (1980) *Scand J Metal* 9:3
54. Petrov AN, Cherepanov VA, Zuev AYu (1987) *Russ J Phys Chem* 61:630
55. Zuev A, Singheiser L, Hilpert K (2005) *Solid State Ion* 176:417
56. Raccah PM, Goodenough JB (1967) *Phys Rev* 155:932
57. Mizusaki J, Tabuchi J, Matsura T, Yamauchi S, Fueki K (1989) *J Electrochem Soc* 208:2:136
58. Sehlin SR, Anderson HU, Sparlin DM (1995) *Phys Rev B* 52:11681
59. Kharton VV, Naumovich EN, Vecher AA, Nikolaev AV (1995) *J Solid State Chem* 120:128
60. Mitberg EB, Patrakeev MV, Lakhtin AA, Leonidov IA, Kozhevnikov VL, Poeppelmeier KR (2000) *Solid State Ion* 130:325
61. Yaremchenko AA, Kharton VV, Viskup AP, Naumovich EN, Tikhonovich VN, Lapchuk NM (1999) *Solid State Ion* 120:65
62. Kharton VV, Naumovich EN, Kovalevsky AV, Viskup AP, Figueiredo FM, Bashmakov IA, Marques FMB (2000) *Solid State Ion* 138:135
63. Petrov AN, Zuev AYu, Vylkov AI (2005) *Russ J Phys Chem* 79:220
64. Tietz F, Schmidt A, Zahid M (2004) *J Solid State Chem* 177:745
65. Petric A, Huang P, Tietz F (2000) *Solid State Ion* 135:719
66. Thornton G, Owen IW, Diakun GP (1991) *J Phys Condens Mater* 3:417
67. Senaris-Rodriguez MA, Goodenough JB (1995) *J Solid State Chem* 116:224
68. Heikes RR (1961) *Thermoelectricity science and engineering*. Interscience, New York
69. Chen CH, Kruidhoff H, Bouwmeester HJM (1997) *J Appl Electrochem* 27:71
70. Petrov AN, Voronin VI, Norby T, Kofstad P (1999) *J Solid State Chem* 143:52
71. Doumerc J-P (1994) *J Solid State Chem* 110:419
72. Raveau B (2004) In: Orlovskaya N, Browning N (eds) *Mixed ionic electronic perovskites for advanced energy systems*. Kluwer, Boston, pp 25–36